Master's thesis

NTNU
Norwegian University of Science and Technology
Faculty of Engineering
Department of Mechanical and Industrial Engineering

Andrea Vågen Edvardsen

Numerical and Experimental Fretting Fatigue Testing Using a New Test Rig

Master's thesis in Mechanical Engineering
Supervisor: Bjørn Haugen
June 2019

NTNU
Norwegian University of
Science and Technology

Andrea Vågen Edvardsen

Numerical and Experimental Fretting Fatigue Testing Using a New Test Rig

Master's thesis in Mechanical Engineering
Supervisor: Bjørn Haugen
June 2019

Norwegian University of Science and Technology
Faculty of Engineering
Department of Mechanical and Industrial Engineering

NTNU
Norwegian University of
Science and Technology

Preface

This master thesis was written during spring 2019 as the final work of the two-year master program of Mechanical Engineering at the Norwegian University of Science and Technology (NTNU). The thesis is a continuation of my specialisation project performed during the fall 2018, where I was introduced to the phenomenon fretting fatigue.

I had no knowledge regarding fretting before august 2018, and the last ten months have been both challenging and exciting. I would like to thank my supervisor Bjørn Haugen for guidance throughout this work. I would also like to thank my co-supervisor Steffen Loen Sunde for taking the time and sharing your knowledge.

Andrea V. Edvardsen

Andrea V. Edvardsen, June 2019, Trondheim

Abstract

Fretting is the term used to describe the condition when contacting surfaces subjected to oscillatory movements in relation to each other experience surface damage. When this condition is kept over time, with cyclic loading, it can lead to fretting fatigue.

This master thesis consists of a literature study that concerns basis knowledge regarding fatigue and fracture mechanics, as well as a more in-depth study on fretting fatigue. The study contains information on the mechanisms and processes of fretting and presents how testing can be performed, the important factors in finite element analyses and some numerical methods that can be used to predict fretting fatigue failure.

The information from the literature study is used to conduct a finite element analysis on a *dovetail* geometry. This geometry is frequently used in turbine blades, where fretting fatigue is a known challenge. These analyses aimed to investigate the stress distribution and stick/slip behaviour in the contact area. The analysis shows a stress concentration at the end of the contact area, which is where the crack is most likely to occur. The results regarding the frictional shear along the contact surface show a stick zone that corresponds to the theory.

Physical tests on a dovetail geometry have been carried out on a new test rig built at NTNU. Two different batches of Al6082 have been tested. The results are promising, but some improvements to the test rig are necessary. Some of the specimens failed due to plain fatigue instead of fretting. As a result of this testing, some improvements have been proposed.

The theory of critical distance (TCD) has been combined with Sines criterion as an attempt to predict fretting failure. The predictions correspond well with the results from the physical testing.

Sammendrag

Fretting er begrepet som brukes til å beskrive tilstanden som oppstår når to overflater i kontakt med oscillerende bevegelser i forhold til hverandre opplever skader i overflaten. Når denne tilstanden holdes over tid, sammen med syklisk belastning, kan dette føre til fretting-utmatting.

Denne masteroppgaven inneholder et litteraturstudie som omhandler basiskunnskap innenfor utmatting og bruddmekanikk, samt et dypere studie om frettingutmatting. Studiet inneholder informasjon om mekanismene og prosessene i fretting, og presenterer hvordan testing kan gjennomføres, hva som er viktig når man benytter elementmetoden og enkelte numeriske modeller.

Informasjonen fra litteraturstudiet er brukt til å gjennomføre en studie med hjelp av elementmetoden på en *dovetail* geometri. Denne geometrien er hyppig brukt i turbinblader, hvor frettingutmatting er en utfordring. Målet med disse analysene er å analysere spenningene og "stick/slip"-oppførselen i kontaktområdet. Modellen viser en spenningskonsentrasjon ved enden av kontaktflaten, det er her en sprekk vil initiere. Resultatene fra skjærspenningene langs kontakten viser en stick-sone som samsvarer med teorien.

Fysiske tester på dovetail geometrien har blitt gjennomført på en ny test rigg bygd på NTNU. To ulike partier av Al6082 har blitt testet. Resultatene fra testene ser lovende ut, men noen forbedringer på testoppsettet er nødvendig. En del av prøvestykkene feilet som følge av utmatting i kjerven i stedet for fretting i kontaktområdet. Som følge av disse resultatene er det foreslått noen forbedringer.

Teorien om kritisk distanse (TCD) er benyttet sammen med Sines-kriteriet for å anta om prøvene ville ryke eller ikke. Resultatene fra antagelsene samsvarer godt med resultatene fra de fysiske testene.

Contents

List of Figures

List of Tables

List of Symbols

2α	Notch Opening Angle
$\Delta\sigma_0$	Plain Fatigue Limit
$\Delta\sigma$	Stress Range
ΔK	Stress Intensity Range
ΔK_{th}	Threshold Value
ν	Poisson's Ratio
$\overline{W}$	Average Strain Energy Density
σ	Stress
σ_0	Critical Stress
σ_a	Stress Amplitude
σ_m	Mean Stress
σ_y	Yield Stress
σ_{max}	Maximum Stress
σ_{min}	Minimum Stress
σ_{uts}	Ultimate Tensile Strength
da/dN	Cyclic Crack Growth Rate
K_C	Fracture Toughness
L	Critical Distance
N_f	Cycles to Failure
S	Magnitude of Cyclic Stress
S_e	Fatigue Limit
W_c	Critical Strain Energy Density
a	Crack Length
E	Young's Modulus
G	Shear Modulus
K	Stress Intensity Factor
P	Normal Load
Q	Tangeltial Force
R	Stress Ratio

Abbreviations

BC Boundary Condition.

CAD Computer Aided Design.

CNC Computer Numerical Control.

COF Coefficient of Friction.

DIC Digital Image Correlation.

EDM Electrical Discharge Machining.

FE Finite Element.

FEA Finite Element Analysis.

FEM Finite Element Method.

FS Fatemi-Socie.

IFEM Infinite Focus Microscope.

LEFM Linear Elastic Fracture Mechanics.

NTNU Norwegian University of Science and Technology.

SED Strain Energy Density.

SEM The Scanning Electron Microscope.

SWT Smith Watson Topper.

TCD Theory of Critical Distances.

1 Introduction

1.1 Background

Fretting is a complex composite phenomena that have been studied for over a century, but still remains elusive. Fretting occurs when contacting surfaces subjected to oscillatory movement in relation to each other experience surface damage. If this condition is kept over time, with cyclic loading, the part can experience fretting fatigue failure. Individually, fretting and fatigue are fairly understood, but the combination, called fretting fatigue, is less understood, and further research is needed.

Fretting fatigue is a widespread problem and has been responsible for a large number of failures across a broad range of applications [1]. Preventing fretting fatigue failure is invaluable for safety-critical industries, such as aerospace and nuclear power generation. A much used example is the "dovetail joint" of compressor blades in turbine engines. It is also a known problem in orthopaedic implants, spline couplings, bolted laps, shrink fits, and other applications where contact between pars is present. Industrial assessments are often based on experience and are sometimes treated as a black box.

Work to further the understanding of fretting and to provide testing conditions has started at the Department of Mechanical and Industrial Engineering at NTNU in cooperation with the industry. The long term aim is to develop a holistic method capable of handling fretting fatigue for practical engineering applications.

The theory in this thesis will to a large extent be based on work performed by D.A. Hills and D. Nowell [1–3] at Oxford University, and a study performed by J.A. Araújo and D. Nowell [4].

1.2 Project description

The aim for this project is to have a working test rig at NTNU, and to provide fretting fatigue data for Al6082. The results from physical testing should be compared with numerical work. To obtain this, finite element analysis (FEA) on the geometry of the test rig will be performed and combined with a fatigue criterion.

1.3 Report outline

The first part of this thesis is a literature study, some of the theory is from the specialisation project performed during the fall 2018. Section 2 will introduce some fundamental concepts regarding fatigue and fracture mechanics. Section 3 gives a more in depth review of fretting fatigue, this includes general theory on the mechanics, testing, and how to predict fretting fatigue through numerical

investigation. This section also includes some important features when using finite element software to analyse fretting.

The second part presents the work performed in this thesis. Section 4 presents the test rig built at NTNU, and how the testing is performed. Section 5 presents the finite element (FE) model used in *Abaqus CAE* and how the theory of critical distance is applied to the model. The results are given in Section 6, and discussed in Section 7.

The last part will make some conclusions based on the results in Section 8, and comment on further work in Section 9.

2 Structural Integrity

This section explains and defines some fundamental concepts concerning the mechanical behaviour of materials.

2.1 Fatigue

The following section is to a large extent based on N.E. Dowling's textbook *Mechanical Behavior of Materials* [5].

When a material or machine component is subjected to repetitive loading, the cyclic stress can lead to microscopic physical damage. This damage, when exposed to continued cyclic loading, can begin to accumulate, turning into a crack and lead to failure. This process can happen at stresses well below the materials given ultimate strength, and is called *fatigue* [5]. In other words, one can say that fatigue failure is failure due to repeated loading, and Dowling reports that up to 80% of all failures in mechanical components is caused by fatigue.

During a fatigue test, a specimen is subjected to a cyclic load varying between σ_{min} and σ_{max}. Stresses above zero are defined as tension, while stress below zero is defined as compression. The terms stress amplitude, σ_a, and mean stress, σ_m, are often used when describing the stress variation. The illustration in Fig. 1 includes the most essential terms in fatigue, and is a pure tension fatigue test as the curve is above the x-axis.

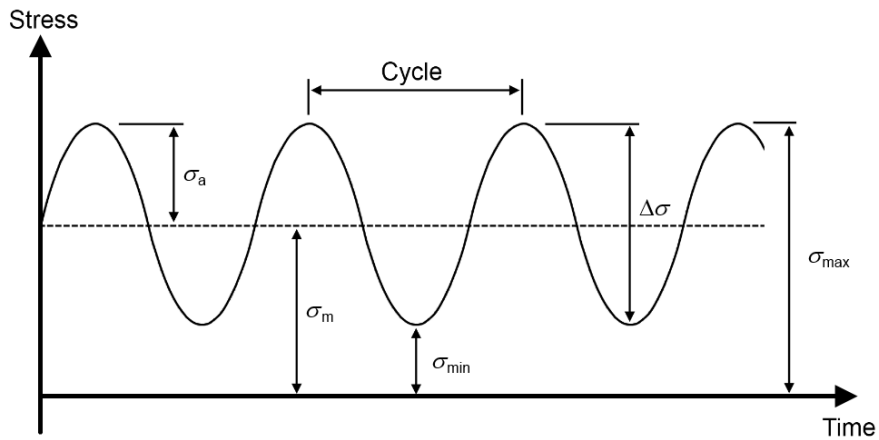

Figure 1: Cyclic loading in a fatigue test

Another important term is the *stress-ratio* (R), which is defined as the relationship between the maximum and minimum stress or load:

$$R = \frac{\sigma_{max}}{\sigma_{min}} = \frac{F_{max}}{F_{min}} \tag{1}$$

When testing fatigue the results are presented in a stress-life curve, also referred to as a S-N curve. Here the magnitude of cyclic stress (S) is plotted against the logarithmic scale of cycles to failure (N_f). This is illustrated in Fig. 2(a). For some materials, e.g., steel and titanium, fatigue tests will reveal a distinct stress level where fatigue failure does not occur. This stress level is labelled S_e and is called fatigue or endurance limit. For other materials, such as aluminium, this limit does not exist, and the term fatigue strength is used. The fatigue strength is defined as the stress level at a particular life, e.g., 10^7 cycles. The S-N curve varies widely for different materials, and is affected by several factors such as mean stress, member geometry, chemical environment, temperature, any processing that changes the mechanical properties or microstructure [5, 6].

When running several fatigue tests at the same load, some scatter will be present. This is due to sample variation in material properties and imperfect control of the test variables. The scatter in log N_f is almost always observed to increase with life [5]. Statistical analysis of the fatigue data enables an average S-N curve to be established.

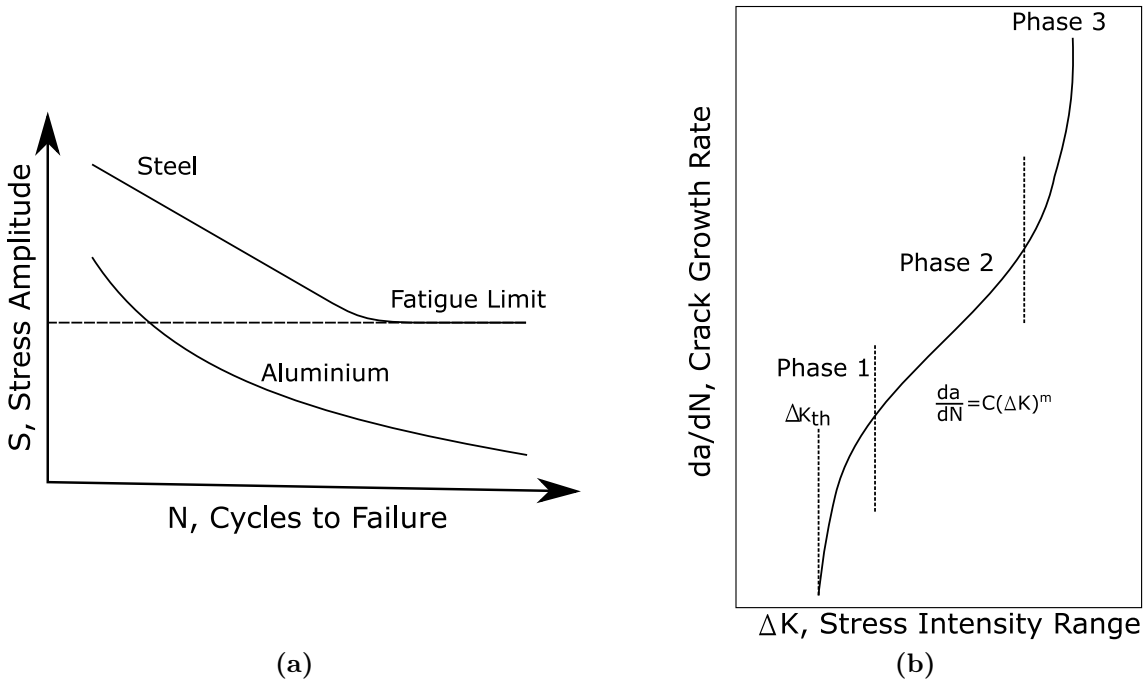

Figure 2: Generic illustration of (a) S-N curve and (b) fatigue crack growth curve

The presence of cracks can drastically reduce the strength of the component. When crack growth occurs due to cyclic loading, it is called *fatigue crack growth*. The prediction of fatigue crack growth is of great importance for large engineered items where safety is important, such as airplanes. The crack growth behaviour is described by the relationship between the cyclic crack growth rate, da/dN, and

the stress intensity range, ΔK. The Paris-law, Eq. 2, gives this relationship.

$$\frac{da}{dN} = C(\Delta K)^m \tag{2}$$

where C is a constant and m the slope on the curve in a log-log plot. A typical plot is illustrated in Fig. 2(b), also showing that crack growth can be divided into three phases. At low growth rates, phase one, the curve is usually steep and approaches a vertical asymptote labelled ΔK_{th}, called the fatigue crack growth threshold. Normally, crack growth does not occur before this limiting value. Phase two is a stable crack growth phase where the Paris-law (Eq. 2) can be applied. At high growth rates, the curve becomes steep again, due to rapid and unstable crack growth just before failure.

2.1.1 Staircase method

When performing fatigue testing, it can be useful to estimate the fatigue limit in advance. The staircase method can be used to provide this estimate. When using this method, the expected stress region of the fatigue limit is divided into stress levels with equal spacing, known as step size (d). This are the dotted lines in Fig. 3. The first specimen can be tested at an arbitrary stress level, normally corresponding to the expected average fatigue strength. The stress level for the next specimen is dependent on the result, if the test leads to failure, the next specimen should be tested at the next-lower stress level. If the test is a run-out, i.e. the specimen did not fail, the next specimen will be tested at the next-higher stress level [7]. This is why the method sometimes is referred to as the "up and down" method.

The initial stress level is typically estimated from experience or preliminary $S - N$ data. By repeating the procedure, the mean value μ and the standard deviation σ can be obtained. The step size is recommended to be as close to σ as possible. To obtain accurate results, 15-30 specimens have to be tested [8].

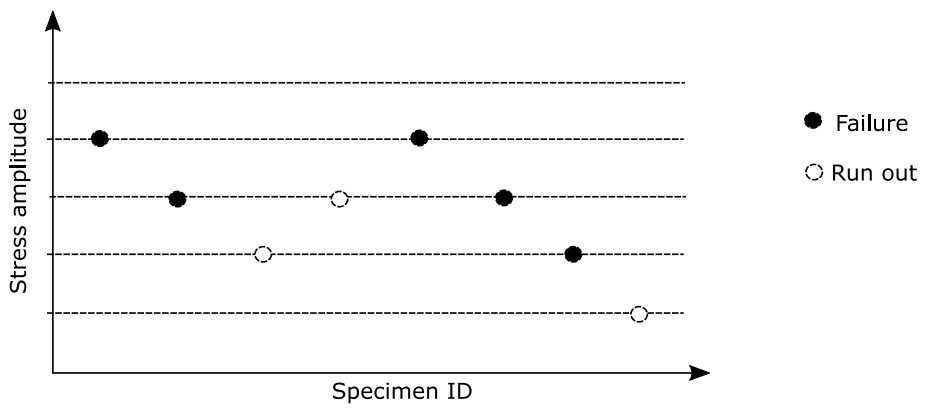

Figure 3: Illustration of the staircase method

When the number of specimens is limited, it is possible to use the *modified staircase method*. In this case, the initial stress level is well below the average fatigue strength. If the test is a run-out the same test specimen is tested again at the stress level that is one increment higher. This is repeated until failure, and then the next specimen is tested at the stress level that is at least two increments lower than the failure-stress for the first specimen. This method should be used with care as some of the results are depending on specimens that already is defined as a run-out.

2.2 Fracture mechanics

This section is based on the text books by N.E. Dowling [5], E.E. Gdoutos [9] and T.L. Anderson's [10].

E.E. Gdoutos [9] states that "fraction mechanics is based on the assumption that all engineering materials contain cracks from which failure starts". A crack in a material leads to high stresses at or near the crack tip, and this area should receive particular attention as this is where further crack growth will occur. In mechanical testing, it is normal to test a notched member to achieve this stress concentration, but for actual engineering applications, fracture may occur in sharp edges due to geometry, welds or small weaknesses from the manufacturing process. There are three types of loading a crack can experience, and the loading situation is often a combination of two or all three. Fig. 4 illustrates the three modes.

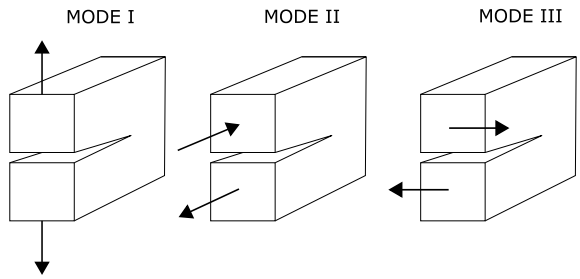

Figure 4: The three basic modes of crack extension

Dowling [5] defines the different modes as listed below:

- **Mode I:** Opening mode, the crack faces move apart
- **Mode II:** Sliding mode, the crack faces slides relative to one another, and normal to the leading edge of the crack.
- **Mode III:** Tearing mode, the faces slide relative to one another, but parallel to the leading edge of the crack

Mode I is caused by tension, while mode II and III are caused by shear loading in different directions. From the theory of fracture mechanics the stress intensity factor, K, can be determined. The factor is usually given a subscript to denote the mode of loading and characterises the magnitude, or intensity, of the stresses in the area around the crack tip in a linear-elastic and isotropic material. For a

crack submitted to mode 1 the stress intensity factor can be expressed as in Eq. 3. A given material can resist a crack as long as K is below a critical value K_C, called the *fracture toughness*. K_C varies widely for different materials depending on temperature, loading rate and member thickness [5]. Failure occurs when $K = K_C$.

$$K_I = \sigma\sqrt{\pi a} \tag{3}$$

Eq. 3 is only valid for semi-infinite bodies where $W \gg a$, W is the width of the member and a the width of the crack. For members that do not fulfil this demand a factor f, which is a function of a and W, is used. If K_I is known, and loading mode I is the only applied load Eq. 4, 5 and 6 can be used to determine the stress situation around the crack tip. Fig. 5 illustrates the stress situation given in polar coordinates around the crack tip. This is valid for Linear Elastic Fracture Mechanics (LEFM) where the plastic zone is assumed to be small.

$$\sigma_{xx} = \frac{K_I}{\sqrt{2\pi r}} \cos\left(\frac{\theta}{2}\right)\left[1 - \sin\left(\frac{\theta}{2}\right)\sin\left(\frac{3\theta}{2}\right)\right] \tag{4}$$

$$\sigma_{yy} = \frac{K_I}{\sqrt{2\pi r}} \cos\left(\frac{\theta}{2}\right)\left[1 + \sin\left(\frac{\theta}{2}\right)\sin\left(\frac{3\theta}{2}\right)\right] \tag{5}$$

$$\tau_{xy} = \frac{K_I}{\sqrt{2\pi r}} \cos\left(\frac{\theta}{2}\right)\sin\left(\frac{\theta}{2}\right)\cos\left(\frac{3\theta}{2}\right) \tag{6}$$

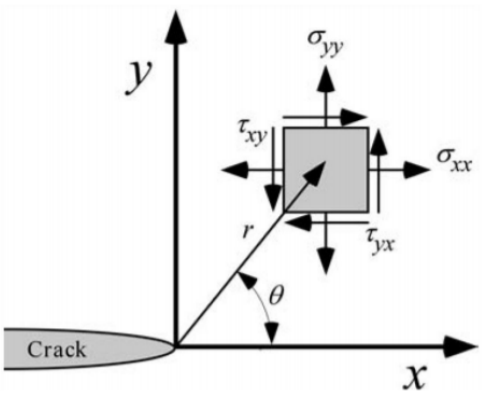

Figure 5: Definition of the coordinate axis given in polar coordinates ahead of a crack tip [10]

Combining theory from fracture mechanics with fretting is especially interesting as it is possible to draw an analogy between the stress concentration in a crack and the concentration at the edge of contact. Giannakopoulos et al. [11] were the first to draw this analogy, this is described in detail in Section 3.3.

2.3 Theory of critical distances

The theory in this section is from David Taylor's book *The Theory of Critical Distances* [12].

The theory of critical distances (TCD) recognises the fact that it is not sufficient to predict failure from the stress concentration at the surface of a notch or crack, called the "hot-spot" approach. To accurately predict failure, it is necessary to have information about the stress field in the vicinity of the notch, as it is known that crack initiation and propagation are strongly influenced by the stress field in this region [13].

TCD is not one single method, but a group of methods that have the use of a material length parameter, called the critical distance L, in common. The method is divided into four groups, where the point method (PM) is the simplest. The slightly more complex methods are the line method (LM), area method (AM) and volume method (VM).

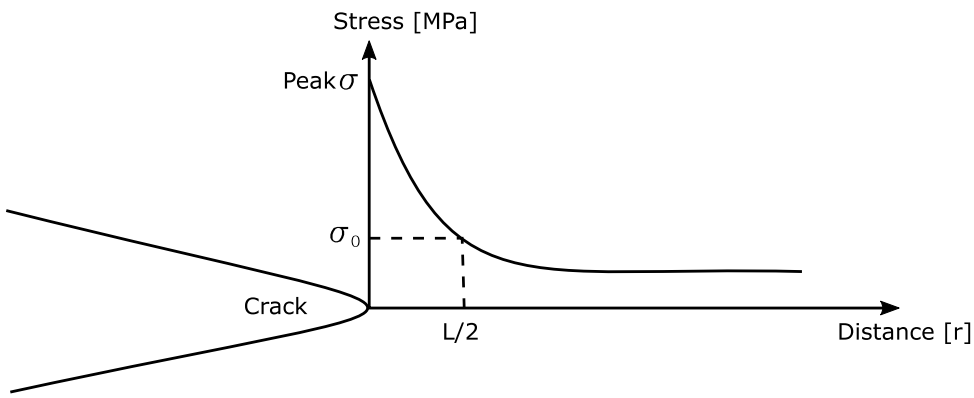

Figure 6: Illustration of point method with stress distribution along a focus path

The theory of critical distance can be applied to situations where the stress field around the stress concentration is known, for example from finite element analysis (FEA). When using TCD two material parameters are necessary, critical stress σ_0 and the critical distance L. When predicting fatigue the stress is cyclic, and the stress range $\Delta\sigma$ is used together with the R-ratio and number of cycles to failure, i.e., the fatigue limit of the material. This will be further explained in section 2.3.1.

Point method

To use TCD one needs a stress-distance curve, this is achieved from FEA along a focus path from the stress concentration, shown in Fig. 6. The point method (PM) uses a failure criterion which D. Taylor [12] states as follows: "Failure will occur when the stress at a distance $L/2$ from the notch root is equal to σ_0". For fatigue failure this can be written as:

$$\Delta\sigma(L/2) = \Delta\sigma_0 \tag{7}$$

It is possible to make a theoretical link between the TCD and linear elastic fracture mechanics (LEFM). The critical distance for the PM can therefore be predicted from Eq. 8 for tensile, and Eq. 9 for fatigue.

$$L = \frac{1}{\pi}\left(\frac{K_c}{\sigma_0}\right)^2 \tag{8}$$

$$L = \frac{1}{\pi}\left(\frac{\Delta K_{th}}{\Delta\sigma_0}\right)^2 \tag{9}$$

Line method
The line method (LM) uses the same focus path as the point method to obtain a stress-distance plot. However, the stress parameter used is the average stress over a distance from $r = 0$. The critical distance is defined as $2L$, and the LM can mathematically be written as:

$$\frac{1}{2L}\int_0^{2L} \sigma(r)dr = \sigma_0 \tag{10}$$

According to Taylor, the differences between the PM and LM are always small, and both methods are applicable for describing experimental data with some scatter.

Area and volume method
The area method (AM) uses the average stress over an area in the vicinity of the notch, while the volume method (VM) uses the volume average. The same value for the critical stress is used for both cases. These methods are more complicated than the PM and LM as the result depends on the shape of the area or volume chosen.

AM and VM are found to give good predictions, but the methods are more complex and do not necessarily lead to an increased accuracy compared to PM and LM. Based the theory presented above, this thesis will focus on the point method

2.3.1 Using TCD to predict fatigue failure

When using TCD to predict fatigue failure, the relevant stress parameter is the plain fatigue limit $\Delta\sigma_0$. TCD is shown to be valid for a wide range of $R-ratios$. Since L is described as a material property, one could expect it to be independent of R but this is not the case. It is known that both $\Delta\sigma_0$ and ΔK_{th} change with R. From Eq. 9 it is showed that L can be determined through these parameters, and is therefore not a constant. This variation is illustrated in Fig. 7. One can see that L decreases slightly from $R = -1$ to $R = 0.5$, before it increases drastically towards $R = 1$. It is important to note that the results in Fig. 7 are somewhat simplified and not followed by all materials, small differences can lead to large changes in the value of L.

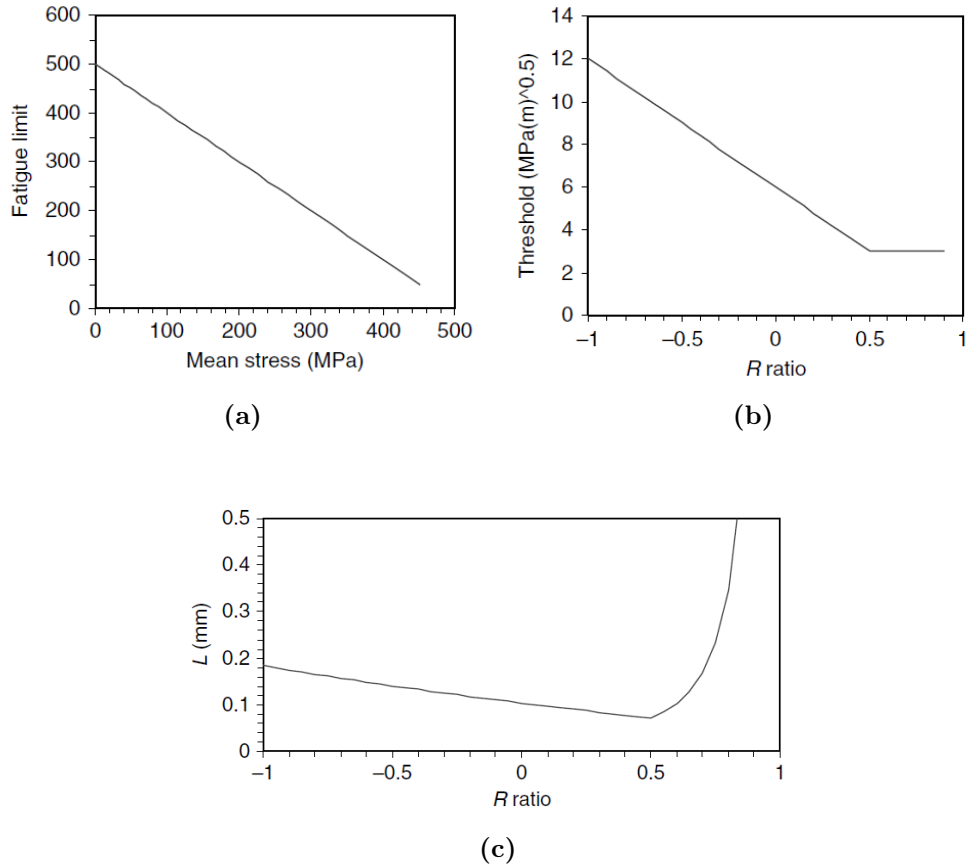

Figure 7: Typical variation of (a) fatigue limit with mean stress and (b) threshold with R ratio. (c) The resulting variation of the calculated value of L with R [12]

2.4 Strain energy density

This section is based on E.E. Gdoutos textbook *Fracture Mechanics: An Introduction.*

The criterion for crack growth under mixed-mode loading was developed by Sih [9] and is known as the strain energy density (SED) criterion. Loads are often not aligned to the orientation of the crack, and in such cases, the stress field around the crack-tip is no longer governed by a single opening mode stress intensity factor K_I, but rather a combination of K_I, K_{II} and K_{III}.

The idea of SED is that the material can be viewed as an assembly of small blocks, and that each block contains a unit volume of material and can store a finite amount of energy. SED is defined as strain energy per volume, shown in Eq. 11. The average SED in a defined control volume around a notch is considered to be the material parameter which describes the initiation of brittle fracture or high-cycle fatigue failure [14].

$$\frac{dW}{dV} = \int_0^{\varepsilon_{ij}} \sigma_{ij} d\varepsilon_{ij} \tag{11}$$

where σ_{ij} and ε_{ij} are the stress and strain, respectively. Critical SED is a failure criterion for tensile stresses, which states that failure will occur when the average value of SED, $\overline{W}$, is equal to a critical value for the average SED, W_c [15]:

$$\overline{W} = W_c \tag{12}$$

W_c is material dependent. If the material is ideally brittle, the critical value can be determined from the ultimate tensile strength σ_{uts}. This gives $W_c = {\sigma_{uts}}^2/2E$ [16], where E is the Young's modulus. In the case of fatigue under mode I loading, the average SED can be calculated from [17]:

$$\Delta\overline{W} = \frac{e_1}{E}\left(\frac{\Delta K_I^N}{R_0^{1-\lambda_1}}\right)^2 \tag{13}$$

where E is the Young's modulus, R_0 the critical radius, ΔK_I^C is the notch stress intensity factor range and e_1 is given by:

$$e_1 = -5.373x10^{-6}(2\alpha)^2 + 6.151x10^{-4}(2\alpha)^{+}0 - 1330 \tag{14}$$

To calculate the SED a control area is used, this area is defined by a critical radius R_0. The radius depends of the shape on the crack or notch, which is illustrated in Fig. 8. For sharp notches and cracks, R_0 is located at the tip of the notch or crack. For blunt notches the centre of the control area is placed at a distance r_0 from the notch tip, which gives a control area given by the radius $R_2 = R_0 + r_0$.

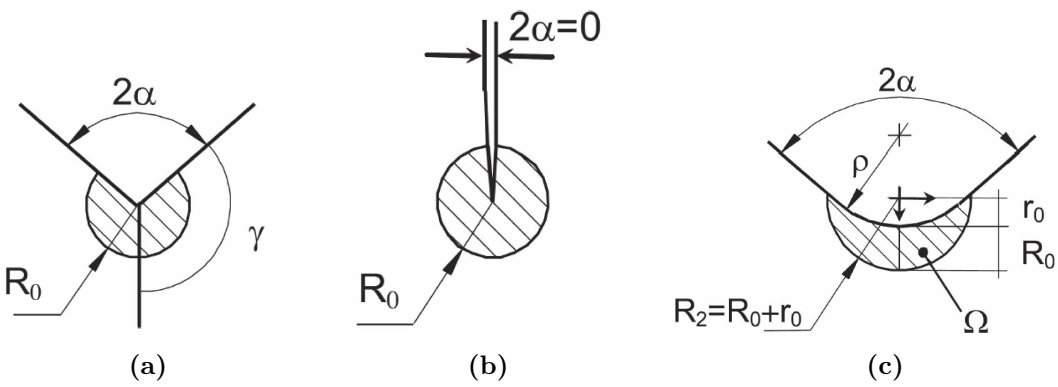

Figure 8: Control area used for strain energy density (a) Sharp notch, (b) Crack, (c) Blunt Notch [16]

The critical radius (R_0) under plane strain conditions is given by [16]:

$$R_0 = \frac{(1+\nu)(5-8\nu)}{4\pi}\left(\frac{K_{IC}}{\sigma_{uts}}\right)^2 \tag{15}$$

where ν is the Poisson's ratio, K_{IC} the fracture toughness and σ_{uts} is the materials given ultimate tensile strength. In the case of fatigue, another calculation for the critical radius has been developed [15]:

$$R_0 = \left(\frac{\Delta K_{IC}^N}{f_1(2\alpha)\Delta\sigma_A^S}\right)^{\frac{1}{(1-\lambda_1)}} \tag{16}$$

where ΔK_{IC}^N is the stress intensity range at the fatigue limit for the notched geometry, $\Delta\sigma_A^S$, is the fatigue limit for a smooth specimen, $f_1(2\alpha)$ is a function depending on the opening angel of the notch and λ_1 is the notch opening parameter for mode I loading.

From Eq. 15 and 16 one can see that the critical radius is dependent on the material properties, for a crack with $2\alpha = 0$ the radius is geometrically independent. Livieri and Lazzarin [17] have reported that a suitable critical radius for aluminium alloys is 0.12 mm.

The results from the SED method is presented in a fatigue $W-N$ curve. One of the biggest advantages with the SED method is that the mesh in finite element analysis can be very coarse as the SED can be derived directly from nodal displacements [16].

2.5 Connecting TCD and SED

It is possible to connect the TCD and SED by combining Eq. 8 and Eq. 15, this is derived through Eq. 17 to 19.

$$L\pi = \frac{K_c}{\sigma_0^2} \tag{17}$$

$$R_0 = \frac{(1+\nu)(5-8\nu)}{4\pi}\left(\frac{K_C}{\sigma_{uts}}\right)^2 = \frac{(1+\nu)(5-8\nu)}{4\pi}L\pi \tag{18}$$

For aluminium with Poisson's ratio $\nu = 0.33$, the relationship becomes:

$$R_c = 0.785L \tag{19}$$

3 Fretting Fatigue

This section will explain the phenomena fretting fatigue, and the features known to influence the process. Different methods for testing and numerical prediction of failure will be described, and important parameters when simulating the process will be identified.

3.1 Fretting fatigue theory

Fretting is the term used to describe the condition when contacting surfaces subjected to oscillatory movements in relation to each other experience surface damage. When contacting surfaces are exposed to this over time, cracks form at the surface and result in fretting. Initially, fretting was recognised as a surface damage phenomenon, what we today call *fretting wear*. Fretting was first described in a paper by Eden et al. [18] in 1911 after detecting debris in the grips of the fatigue test machine, interpreted as surface wear or corrosion. Over the years, the combination of fretting contact and fatigue loading were found to be critical.

To understand fretting fatigue, one needs to understand both fatigue and contact theory. D.A. Hills and D. Nowell at Oxford University are two of the most prominent researchers on fretting fatigue, and this section will to a large extent be based on their research.

Fig. 9 shows two bodies brought into contact by an applied normal force, P, and a tangential force, Q. The primary area of concern in fretting is the area shared by the two contacting bodies, between the dotted lines shown in the figure.

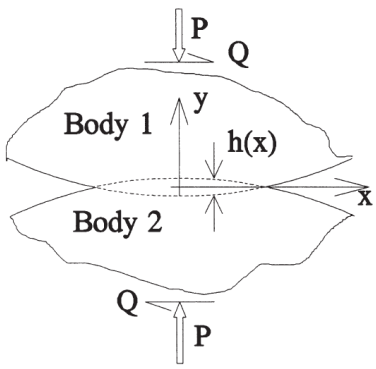

Figure 9: Line contact between two elastically deformable bodies subject to a normal force (P) and a tangential force (Q) [2]

Fretting fatigue is usually separated into different stages. The first stage often involves wearing off the oxide layer on the surface. When this layer is worn off, cold-welds forms at the surface and causes an increase in the coefficient of friction. Continuing to load the surface after the first phase, the micro-welds will break, and wear debris will form. Additional loading cycles may induce plastic deformation and

add microcracks to the surface [19]. The crack initiation process is highly dependent on the material microstructure.

Compared to plain fatigue, fretting fatigue displays a number of features that must be considered in any analyses, both in experimental results and design situations. D. Nowell et al. [1] point out four important features:

(i) Stress gradients are likely to be very high due to the localised stress concentration at the contact area

(ii) Loading is likely to be non-proportional around the contact point

(iii) Initiated cracks will experience a variable R-ratio as they grow away from the contact

(iv) Localised surface damage at the asperity level may play a role in accelerating the initiation of cracks

Item (i) is especially important as the magnitude of stress gradients at the contact usually is much higher than those associated with design features, i.e. holes and notches. This will lead to a stronger size effect. R. Bramhall, at Oxford University, was the first to investigate the size effect systematically [3]. He noted that the peak pressure is related to the normal load, P, and the pad radius, R, in a cylindrical Hertzian contact by:

$$p_0 = \sqrt{\frac{PE^*}{\pi R}} \quad \text{and} \quad a = \sqrt{\frac{4PR}{\pi E^*}} \tag{20}$$

where E^* is a constant for the material, and a is the semi-width of the contact. This model, using Hertzian contact is often referred to as the Cattano-Mindlin model. From Eq. 20 it is clear that p_0 is proportional to $\sqrt{P/R}$, while a is proportional to $\sqrt{PR}$. Because of this, it is possible to vary the extent of the contact and the associated stress field, while keeping the magnitude of the stress constant. The situation is in reality a bit more complicated, but experiments show that there is a clear variation in fatigue life with variation in contact size [3, 4].

As the contact edge gets sharper, ending with complete contact, the Hertzian stress analysis fail and singularities arises. This is why the shape of the two contacting surfaces also is an important factor.

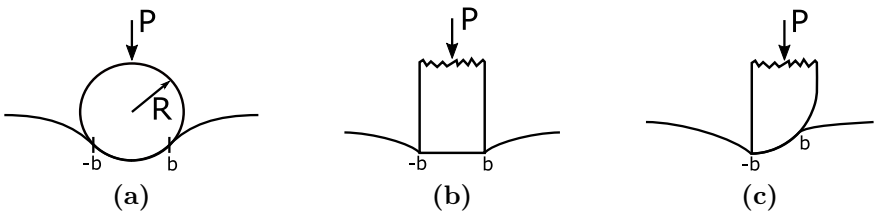

Figure 10: Characterisation of contact. (a) Incomplete, (b) complete, (c) incomplete but with singularities [2]

D.A. Hills [2] describe the differences between *complete* and *incomplete* contact in the following way. If a cylinder pressed into an elastic half-plane as in Fig. 10a the contact width will increase with an increase in pressure. This is an example of *incomplete contact* where the contact size is dependent on the applied load. With incomplete contact, the contact pressure distribution is locally disturbed by minor imperfections in the surface finish. In contrast we have *complete contact*, illustrated in Fig. 10b, where the size of the contact is independent of load. While the two bodies with incomplete contact have a common tangent at the edge of the contact, is this not the case for complete contact. The slope of the surface of the half-plane is not continuous at the edge of contact, which means that the corresponding contact pressure is *singular*. In this case, even a minor manufacturing flaw can change the pressure distribution largely.

It is possible to have a combination of the two different contact situations with a D-shape, illustrated in Fig. 10c. Here, the contact pressure will be singular in $-b$, but fall to zero in b. Thus, complete and incomplete contact are fundamentally different by the theoretical singularity due to sharp edges at complete contact. This edge will, in reality, have a finite radius and plasticity will relieve the stress.

Independent of the geometry it is frequently the case that the most highly loaded point is at or near the edge of contact [1]. As the pressure falls to zero, the coefficient of friction required to prevent slip has to be infinite. Therefore it is inevitable that some slip occur if a Hertzian contact is loaded. Fig. 11 illustrates the stick and slip regions of Hertzian contact, with the stick zone from $-c$ to c. Due to existence of high shear traction at the edge of contact, it is reasonable to suggest that slip may take place at the contact end as well [2].

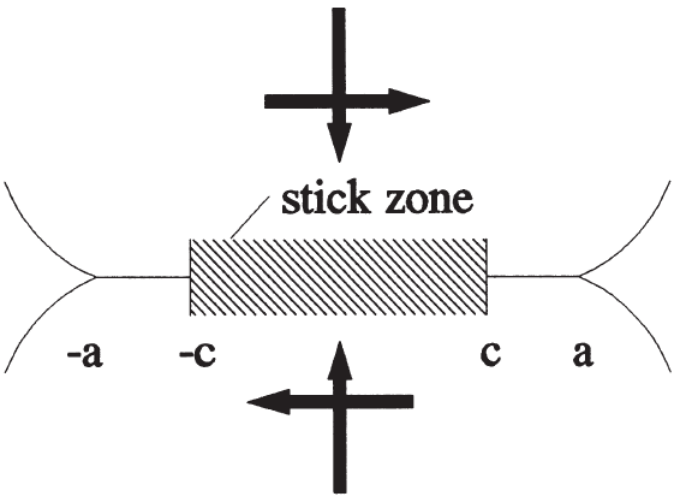

Figure 11: Illustration of stick and slip regions [2]

3.1.1 Fretting maps

It is a challenge to reproduce the small relative displacement occurring during fretting under laboratory conditions, and a number of visual descriptions of fretting have been researched using fretting maps. A fretting map uses numerical and experimental data to find the critical displacement amplitude and tangential force values for the transition from one fretting regime to another. Today fretting maps are used to describe the overall fretting behaviour and is a useful tool in early design processes.

Vigsbo and Söderberg [20] suggested a fretting map displaying four different regimes:

(i) Stick regime

(ii) Mixed stick-slip regime

(iii) Gross slip regime

(iv) Reciprocating sliding regime

In the *stick regime* there is low surface damage by oxidation and wear. In this regime, one experience low fretting damage and no fatigue crack growth is observed. For the *mixed stick-slip regime* wear and oxidation effects are present but small. The damage in this regime is identified as fretting fatigue. The *gross slip regime* shows severe wear damage, but crack formations are limited. In the gross slip regime, the contact surfaces can be in full sliding across each other, and the damage related to this is often identified as fretting wear. In the *reciprocating sliding regime* the gross slip approaches reciprocating sliding and leads to sliding wear.

By combining numerical data with literature the fretting-map in Fig. 12 was suggested. For low amplitudes, in the mixed stick-slip regime, the wear rate is very low. When entering the gross slip regime the wear rate increase drastically until it levels-off in the reciprocating sliding regime. Several studies have shown that the fretting fatigue life decreases with increasing amplitude up to a certain value [20].

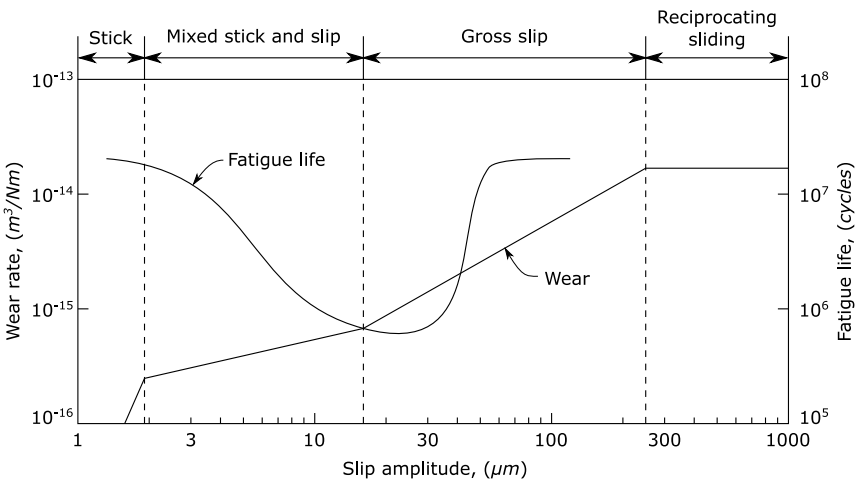

Figure 12: Relating the slip amplitude to fretting regime [20]

The governing regime is visible in the hysteresis loop, illustrated in Fig. 13, where a small area between the lines represents partial slip and a large area represent gross sliding [21].

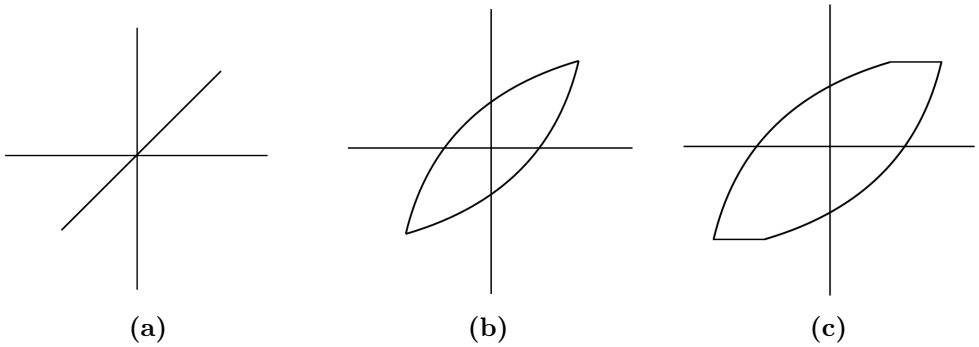

Figure 13: Hysteresis loop for (a) sticking, (b) partial slip and (c) gross sliding

3.1.2 Fretting wear

Wear caused by fretting occurs in both partial slip and gross sliding regimes. Fretting wear is, in the same way as fretting fatigue, a challenge in engineering components such as hip joints and dovetail blades due to the continuous change of contact surfaces. Wear is hard to measure in physical experiments, and this is why FEM is used to predict the process.

When using the finite element method (FEM) there is always a balance between accuracy and efficiency, and the model of fretting wear is usually simplified. One of the common simplifications is that the coefficient of friction (COF) is kept constant [22]. The coefficient of friction is known to change during fretting [23], and should be considered as a system dependent property rather than a simple material constant [24]. This is because of the sensitivity to sliding distance and the environment.

Yue and Wahab [25] performed a study on fretting wear with two different models, constant COF and variable COF. The results showed that in gross sliding regimes the effect of using a variable COF had low impact on the wear volume at the end of the steady state. However, for partial slip or the running in stage of gross sliding, the models with variable COF turned out to be closer to the experimental results.

3.2 Fretting fatigue testing

There have been a number of different test setups over the years. However, no universal standard for how testing should be performed is existing, and there is still many different setups. This section will describe some of the various setups over the years.

One of the pioneers on experimental work on fretting fatigue was Robert Waterhouse. He built a bridge setup shown in Fig. 14, where a pair of bridge shaped devices was clamped on to the specimen using a proving ring. The setup is simple, enabling the use of normal fatigue specimens, either in a bending or cyclic tension test. The biggest problem with this test setup is the fact that the condition at each foot (point A and B) will not be identical, and it is likely that one foot will slip before the other [1].

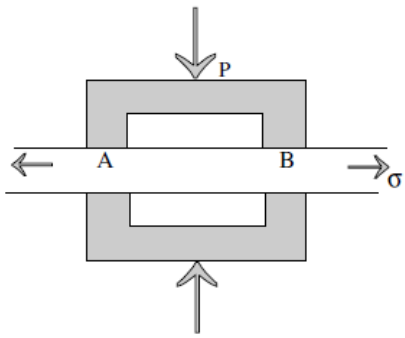

Figure 14: Bridge fretting test [1]

In the late 1960s and early 1970s Nishioka and Hirakawa built a new apparatus to avoid the problem with singularities due to complete contact. This was solved by introducing Hertzian contact with cylindrical pads clamped against a flat specimen. The geometry has been later adopted by several researchers, including John O'Connor and his student Bramhall at Oxford University. Fig. 15 illustrates the setup.

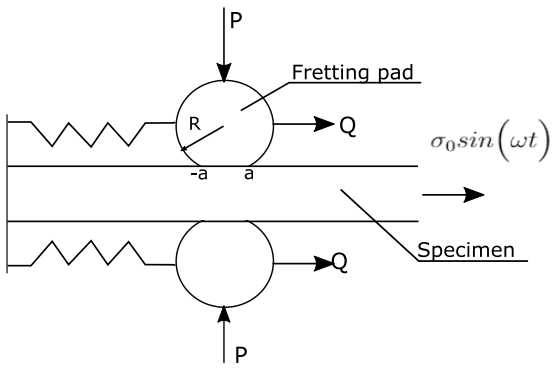

Figure 15: Fretting fatigue test using Hertzian contact [3]

The apparatus uses one single actuator to provide both bulk and shear loading. This setup enables a full description of the contact conditions and the state of stress. It was with this apparatus they verified that the contact size had great impact on fretting fatigue performance. The biggest advantage with this setup, and probably why it have been repeated all over the globe for decades, is the economic perspective. The apparatus only requires one single actuator and a frame, but the corresponding disadvantage is that there is a practical limit due to the use of a spring to apply the tangential load.

There have been conducted experiments where the geometry is more related to the actual component. The dovetail geometry is one of the most researched geometries in fretting fatigue. Ruiz et al. [26, 27] developed an apparatus for testing this geometry, shown in Fig. 16. The blade loads, representing the centrifugal force in the engine, are applied to two separate and opposing dovetail specimens. The specimens are placed in a central disk, which is subjected to load, simulating disk expansion under centrifugal load. This is an important feature because it allows accurate representation of relative slip in the engine. Several similar test-setups have been tested over the years, e.g., by P. Golden in cooperation with others [28–30].

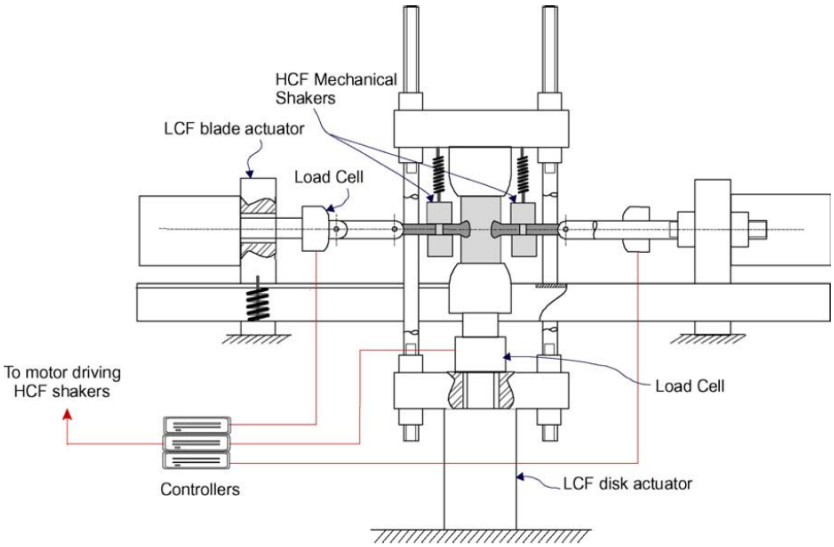

Figure 16: Dovetail setup by Ruiz, placed at Oxford

A more general apparatus was developed later on, shown in Fig. 17. This apparatus uses two colinear and separate actuators, one for bulk tension and one for shear force. This permits independent control. The apparatus was intended to use Hertzian contact, but ended up with complete contact. Further developments has been done, and today the apparatus consists of three separate servo-hydraulic actuators, giving the possibility for all three loads to be imposed separately. To this date, no results from this general test-setup has been published. This new setup will open up a whole new area for researching fretting fatigue, according to D. A. Hills [3].

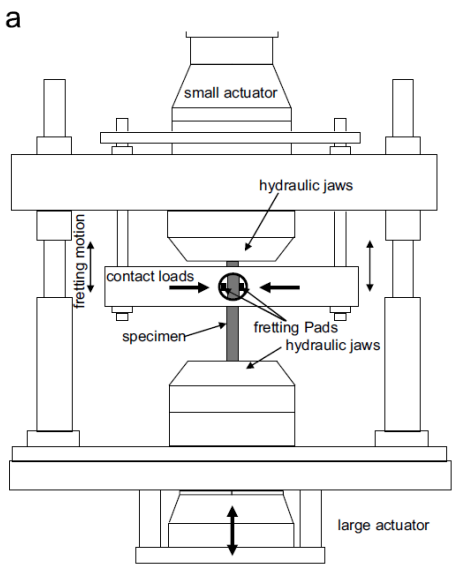

Figure 17: Two collinear actuator fretting fatigue apparatus schematic [3]

This section only describes the most common methods for testing, and there are many other variants. Early tests were conducted only to gather information about the features involved with fretting. In 1992 there was an attempt to start standardisation of fretting fatigue testing. However, there is no generic standard up to this date [31]. The American ASTM E2789 - 10 standard [32] only includes guidelines and general requirements for conducting a fretting fatigue test. Even though there is no generic standard, the Japanese scientists developed a standard, JSME S 0-15-2002, in 2002 [31]. In this standard they recommend the bridge setup shown in Fig. 14, and critical dimensions for the fatigue specimen and fretting pads are suggested.

3.3 Predicting fretting fatigue

There has been put much effort into predicting fretting fatigue in engineering design. This section will take a brief look at some of the different methods. Due to the complicated nature of fretting fatigue, predictions in early design processes is difficult. This is probably why there have been so many different models applied to the prediction of fretting fatigue, and research is still ongoing.

Empirical parameters
In the early attempts on predicting fretting fatigue special empirical parameters were employed. One of the most popular parameters, suggested by Ruiz [26], was formed from the product of the local slip amplitude and the maximum shear traction ($\delta\tau$). This was later enhanced to include the maximum local stress component parallel to the contact surface ($\delta\tau\sigma$). The enhanced parameter was found to provide a better estimation of the location of fretting crack initiation, but still unlikely that a critical value of either parameter could work as a material constant.

Critical plane
There have been attempts to apply simple fatigue parameters such as the Fatemi-Socie (FS) and Smith-Watson-Topper (SWT) parameters to the fretting problem [1, 4]. Because of the multiaxial nature of the stresses, critical plane-based methods have been attempted to predict the fretting fatigue limit. For FS the plane having the maximum shear is considered the critical plane, while in SWT the critical plane is based on tensile stress. The FS and SWT critical plane parameters are given in Eq. 21 and Eq. 22 respectively. The right part of the equations are obtained from combining the criterion's with Coffin-Manson and Basquin's law.

$$FS = \frac{\Delta\gamma}{2}\left(1 + \alpha\frac{\sigma_{max}}{\sigma_y}\right) = \frac{\tau'_f}{G}(2N_f)^{b_0} + \gamma'_f(2N_f)^{c_0} \tag{21}$$

where $\Delta\gamma$ is the shear strain range during the cycle, σ_{max} is the maximum normal stress, σ_y is the yield stress, G is the shear modulus and α, τ'_f, γ'_f are material related parameters. b_0 and c_0 are the shear fatigue strength and shear fatigue ductility exponent respectively.

$$SWT = \frac{(\sigma'_f)^2}{E}(2N_f)^{2b} + \sigma'_f\epsilon'_f(2N_f)^{b+c} \tag{22}$$

where σ'_f and b are the material fatigue strength and exponent, ϵ'_f and c are the fatigue ductility coefficient and exponent, respectively. E is the modulus of elasticity and N_f is the number of cycles to initiate a crack with a given length.

It is known that shear based parameters work better for ductile materials, and tensile based parameters for brittle materials [33]. Normally it is difficult to know the dominant mode of crack initiation in advance, and this makes the choice of criterion difficult. A conservative approach may be to calculate both FS and SWT and use the worst case, as suggested by Araùjo and Nowell[4].

Notch analogies
There have been attempts to draw a line between fretting fatigue and the theory of notch fatigue. If the stress concentration is at the edge of contact, and the contact is incomplete, the normal (P) and shear (Q) tractions will fall to zero, and the only non-zero component will be the stress gradient parallel to the surface [2]. Using the illustration in Fig.18 and the assumptions mentioned, it is possible to draw an analogy between the stress state for the contact and a notch. It is a loose analogy, but good results can be achieved by varying the notch size, root radius, opening angel and remote load [1]. The approach has its uses, but because of the high stress gradients present, compared to notches, it is unlikely that standard values for notches can be used.

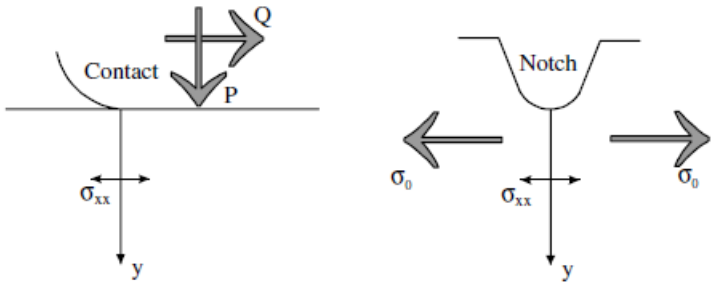

Figure 18: Analogy between stresses at contact and notch [1]

Crack analogies have also been suggested, drawing the analogy between the singular stress field at crack tips with the singularity in sharp edged contact [11, 34].

Theory of critical distance

There have been some attempts to use the TCD to fretting [12]. Fig. 19 illustrates the fretting process, where the focus path should be placed along y'. D. Taylor states in 2007 that there only have been a few investigations on fretting fatigue using TCD, but it is sufficient to suggest that TCD may be a useful tool [12].

Vallellano et al. [35] estimated the local stress field using an analytic solution. The material constants were found in literature, and the critical distance were calculated the normal way for both the point and line method, as described in Section 2.3. Both methods gave good results, with errors of the order of 10% [12].

Araújo et al. [36, 37] applied TCD to the previously published data from the study performed by themselves in 2002 [4]. They combined the TCD with different critical plane approaches, with good results. The results regarding the TCD is promising, but further research is still necessary.

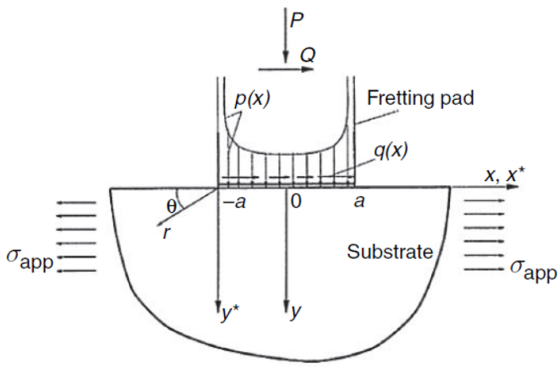

Figure 19: Illustration of fretting from Taylor [12]

3.4 Using FEM to predict fretting fatigue

The finite element method (FEM) has become an essential tool for engineers. Depending on which solver one uses, the FEM can be an excellent tool for solving problems such as structural analysis, fluid flow, dynamic problems. When modelling and analysing engineering design one usually have a complex geometry and loading situation. Complex geometry and loading requires a fine mesh, and a fine mesh leads to long simulation time. To reduce the simulation time it is possible to use sub-modelling techniques. Thus, in this case the local features governing fretting fatigue crack initiation can be separated from the global solution. This way, detailed analysis can be performed for the mechanical fields relevant for fretting, isolated from the rest of the model.

In this thesis *Abaqus CAE* will be used as the finite element (FE) tool.

3.4.1 Mesh

When analysing in FE-software it is important to use the correct element type and size to obtain correct results. In *Abaqus* there are several types of elements, and which to choose depends on the geometry and stress distribution. When meshing a 2D model one have two element types "quad", Fig. 20(a), or "triangular", Fig. 20(b). Generally quad elements has better convergence rate than the triangular, but triangular is better for complex geometries.

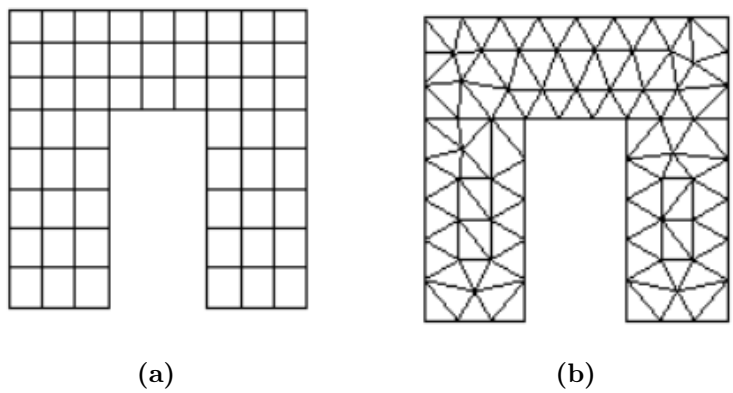

Figure 20: Element types for 2d models (a) quad elements and (b) triangular elements

It is important to use a sufficiently refined mesh to ensure that the results are close to reality, but smaller elements can significantly increase the computational cost. Due to this, it is normal to use a fine mesh in the critical areas, while the rest of the model has a more coarse mesh. To control the mesh quality one often perform a mesh convergence test to check that the different meshes give essentially the same result. It is important to keep in mind that sharp corners in a finite element model will result in a stress singularity, and such singularities will in a linear-elastic model cause the stresses to diverge.

3.4.2 Contact formulations

When analysing fretting fatigue it is important to use the correct parameters and properties to obtain good results. However, it is challenging to define the contact correctly. When defining contact in *Abaqus* the standard is either "General contact" or "Surface-to-surface contact". Due to the complex nature of fretting, surface-to-surface is the preferred choice. For this interaction, there are two possibilities:

- **Node-to-surface**: Connecting a slave node to a master surface, normally used when modelling a sharp object, e.g a pin, to a surface
- **Surface-to-surface:** Connecting a slave surface to a master surface, here the shape of both the slave and master surface is considered. Normally used when modelling contact between two bodies moving relative to each other.

In general, surface-to-surface interaction provides a more accurate stress result than node-to-surface [38]. Fig. 21 from *Abaqus User Manual* shows the improvement in accuracy for the stress distribution with surface-to-surface contact compared to node-to-surface contact. In node-to-surface contact the forces tend to concentrate at the slave nodes, and this leads to peaks in the stress distribution and therefore gives an overestimation.

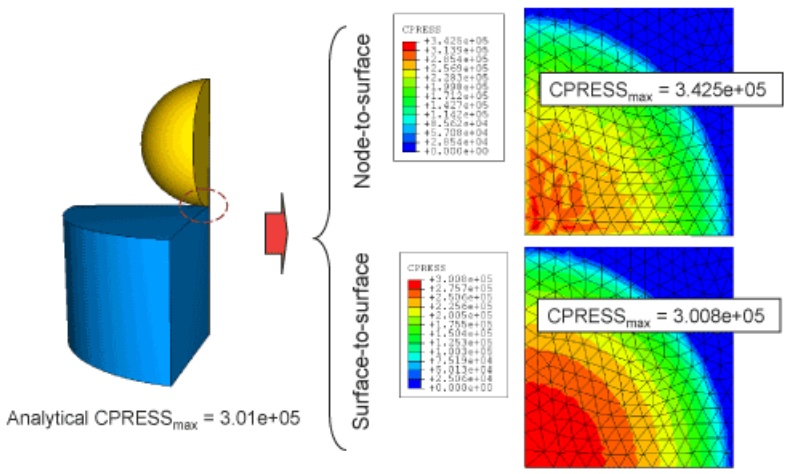

Figure 21: Stress distribution with surface-to-surface and node-to-surface contact [38]

When the contact type is decided, the contact properties have to be specified. All information is obtained from *Abaqus User's Guide* [38].

- **Small or finite sliding:** in small sliding there will be relatively little sliding of one surface along the other, although the two bodies may undergo large motions. Finite sliding is the most general and allows for any arbitrary motion of the surfaces.

- **Tangential behaviour**
  - *Friction formulation:* the standard choices are "Frictionless", "Penalty" or "Lagrange multiplier". The differences will be described in section 3.4.3.
  - *Coefficient of friction:* the coefficient of friction have to be specified, depending on the material and environmental conditions. In fretting it is likely that the coefficient will change during cyclic loading, which makes it difficult to choose a correct value.
- **Normal behaviour**
  - *Pressure-overclosure:* this parameter decides how the surfaces behave to each other. The standard choices are "soft contact" or "hard contact". Hard contact gives a behaviour where the bodies are prevented from penetrating each other, how strict the "no penetration" is depends on which "constraint enforcement method" one uses.

3.4.3 Friction formulation

When analysing fretting problems in *Abaqus* there are, as mentioned, three choices for friction formulation. Friction is known to have a great impact on fretting, and *Frictionless* is therefore not the appropriate choice.

The *penalty method* is illustrated in Fig. 22. To impose $u_2 = u_6$, the nodes u_2 and u_6 are connected with a *penalty element*, element (7). This element will use the connected nodes to describe the stiffness and placement, and therefore the number of degrees of freedom is kept the same. The main advantage with this method is the straightforward computer implementation. Once all elements are assembled, the system can pass on to the equation solver. With this method, the contact force is proportional to the penetration distance, and this leads to some degree of penetration.

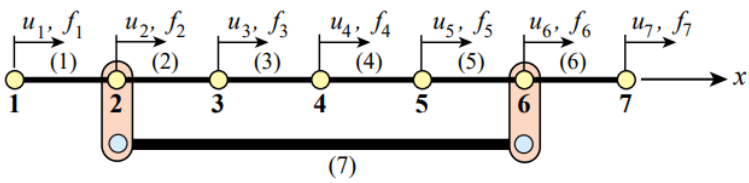

Figure 22: Penalty method with "penalty element" of axial rigidity

Abaqus offers both linear and nonlinear variations of this method, but the default penalty method is linear. The penalty stiffness is by default set to 10 times a representative underlying element stiffness [38]. The contact penetrations resulting from this stiffness will not affect the results in most cases, but these penetrations can contribute to some degree of stress inaccuracy if the model has a rough mesh or with displacement-controlled loading.

The *Lagrange multiplier method* is illustrated in Fig. 23. To impose $u_2 = u_6$, a reaction force pair, $\lambda, -\lambda$, is added to node 2 and 6. This force is called a *Lagrange multiplier* and is unknown. This requires an expansion of the original stiffness matrix due to the increase in degrees of freedom.

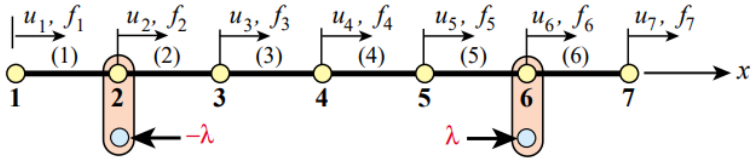

Figure 23: Lagrange multiplier method with force-pair λ that enforces $u_2 = u_6$

Lagrange multiplier gives a more accurate result, but also adds significantly to the solution cost. The main advantage compared to the *penalty method* is that it captures the sticking conditions where the relative motion is zero, while for *penalty* the sticking is approximated with a penalty stiffness. Any *Lagrange multiplier* associated with contact is only present for active contact, this means that the number of equations will change as the contact status changes. The additional degrees of freedom usually increases the number of iterations required to obtain a converged solution, and sometimes even prevent convergence due to presence of rigid constraints [38]. Because of the added simulation time when using this friction formulation, it should only be used in problems where the solution of stick/slip behaviour is important, such as fretting.

4 Experimental Work

4.1 Test specimens

The geometry of the test specimens is illustrated in Fig. 24. The upper part is 40 mm wide, this is to be sure that failure does not occur in the area around the hole. The contact area has an angle of 40 degrees to the horizontal axis.

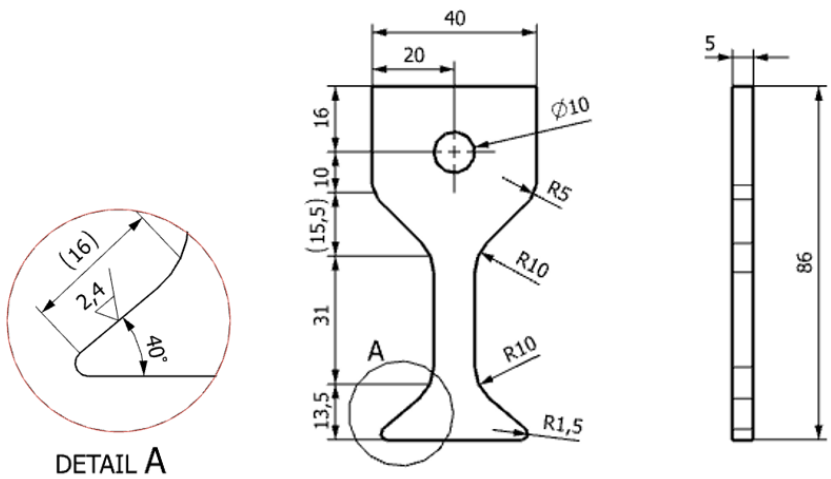

Figure 24: Illustration of test specimen

Two different materials will be tested, the specifications are listed in Table 1.

Table 1: Material data for test specimens

Material	Young's modulus (GPa)	Poisson's ratio	Mass density (g/cm^3)	Yield strength (MPa)
Al 6082-T6*	70	0.33	2.7	318

* Datasheet for material can be found in Appendix A

4.1.1 Sample preparation

CNC milling machining
The first batch of Al6082 is produced at the department of Mechanical engineering at NTNU. The specimens are produced by Computer Numerical Control (CNC). In this production method a computer converts the design from CAD to numbers that can be considered as coordinates for the movement of the cutter. The CNC machining and conventional machining gives the same end product, but CNC has some advantages regarding production time and accuracy. The Al6082 specimens are produced from a 5 mm rolled plate, and the methods give a smooth surface finish.

Wire Electrical Discharge Machining

The second batch of AL6082 is produced by Wire Electrical Discharge Machining (EDM). This EDM method uses a wire which acts as an electrode to remove material by series of discrete sparks between the work-piece and the wire. The method is extensively used in aerospace and automotive industries due to its capability of producing complex shapes. The thermal material removal generates a heat-affected zone on the surface, creating sub-layers. The most important layer is called the white layer, this is leftover molten material that re-solidifies on the surface through the cooling face. This leads to a rougher surface than with other machining methods, such as milling. The existence of this white layer is considered to have a negative impact on the life of parts machined by EDM [39]. The method may lead to small microcracks in the surface which can initiate crack growth, and is known to affect the fatigue life. An increase in surface hardness for machine components produced by EDM has also been reported [40], this is related to the heat created through the production.

The Al6082 specimens have quite a rough surface, and this may influence the fretting process. By using an Alicona Infinite Focus Microscope (IFEM) the surface is investigated. Fig 25(a) gives a microscope-picture of the contact surface of the dovetail, while Fig. 25(b) gives a better illustration of the surface roughness. Fig. 25(c) shows the variation of height for a cross-section in the 3D plot. From these results, the mean peak to valley height of roughness is measured to be approximately $R_z = 24.1\mu m$, and the average roughness of the profile is $R_a = 4.5\mu m$.

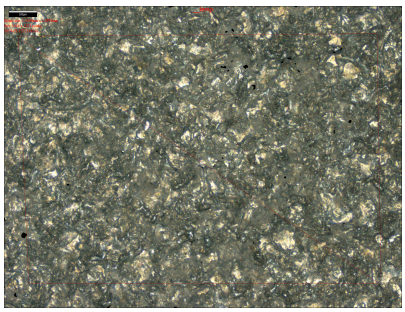

(a)

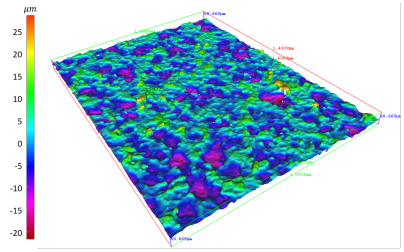

(b)

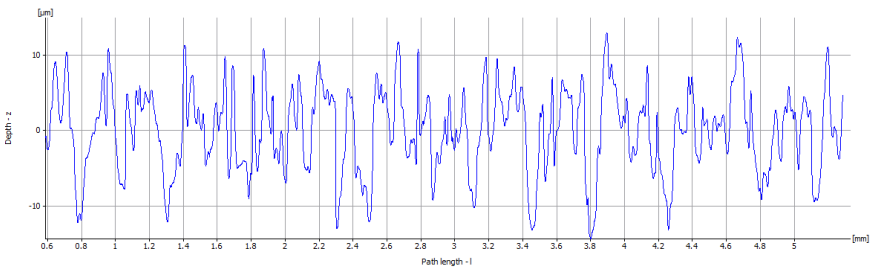

(c)

Figure 25: (a) Picture of the surface and (b) illustration of surface roughness of contact area for test specimen, (c) profile of cross-section

Preparation for microscope

To be able to analyse the microstructure after testing, the specimens need to be prepared. The dovetail root is cut from the rest of the specimen using the *Struers Accutom-5*0 cutting machine. The specimens are hot-mounted in PolyFast, and polished. The polishing is performed in steps. Starting with grinding papers with roughness P220 - P500 - P1000 - P2000, and then polished with SiH paper and diamond paste, down to a finale grind size of $1\mu m$. The sample is rinsed with ethanol to remove the redundant diamond paste. The sample needs to be etched according to standard, this is not yet performed. The prepared specimens are shown in Fig. 26. The samples can be examined using both an optical microscope and scanning electron microscope SEM.

Figure 26: Polished test specimens mounted in PolyFast

4.2 Fretting fatigue test rig

A new test rig has been build at NTNU, inspired by the well known dovetail geometry [28, 29, 41]. The setup consists of 5 parts, a universal joint, the test specimen, two fretting pads and a fixture. The universal joint and the lower fixture is clamped into the testing machine, the size of the grip area is made in a way that permits the setup to be used in several fatigue machines. The test specimen is attached to the universal joint by a bolt. The fretting pads are made separate from the lower fixture to be able to change them when they get worn, and to be able to vary the radius, material and coating. The fretting pads are slid into place and kept at the correct position by pressure from the test specimen.

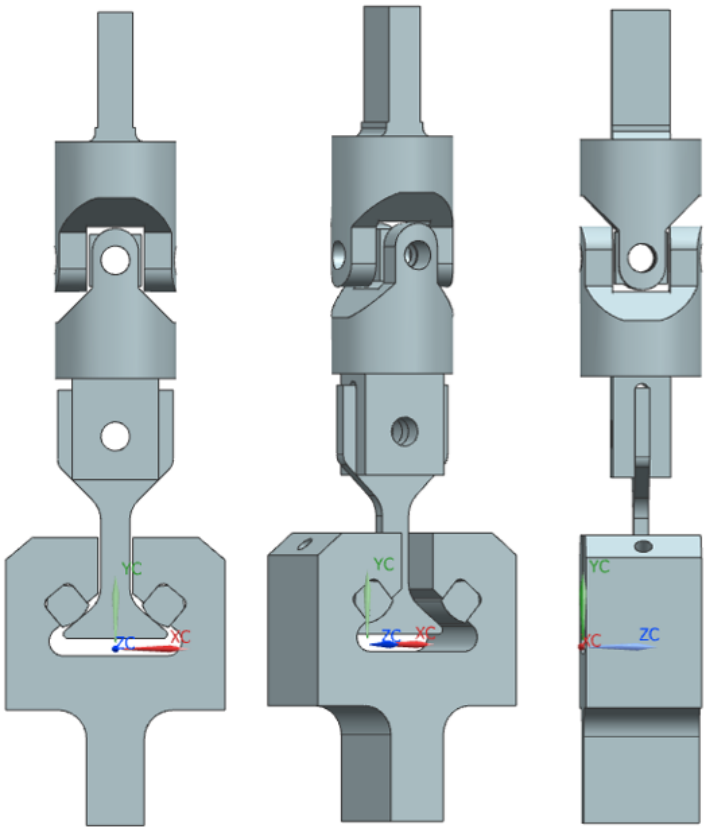

Figure 27: Illustration of test setup from Siemens NX

The setup is made in a way that enables testing of two specimens at the same time. This is done by attaching the test specimens on each side of the universal joint, instead of in the centre. This can be useful but requires high accuracy as it is hard to ensure that both specimens are properly aligned.

End caps can be used on both sides of the fixture, closing the chamber and allowing for testing in submerged conditions. This can be useful e.g., for orthopaedic implants as the body fluids are expected to impact the fretting mechanisms due to the corrosive environment [42].

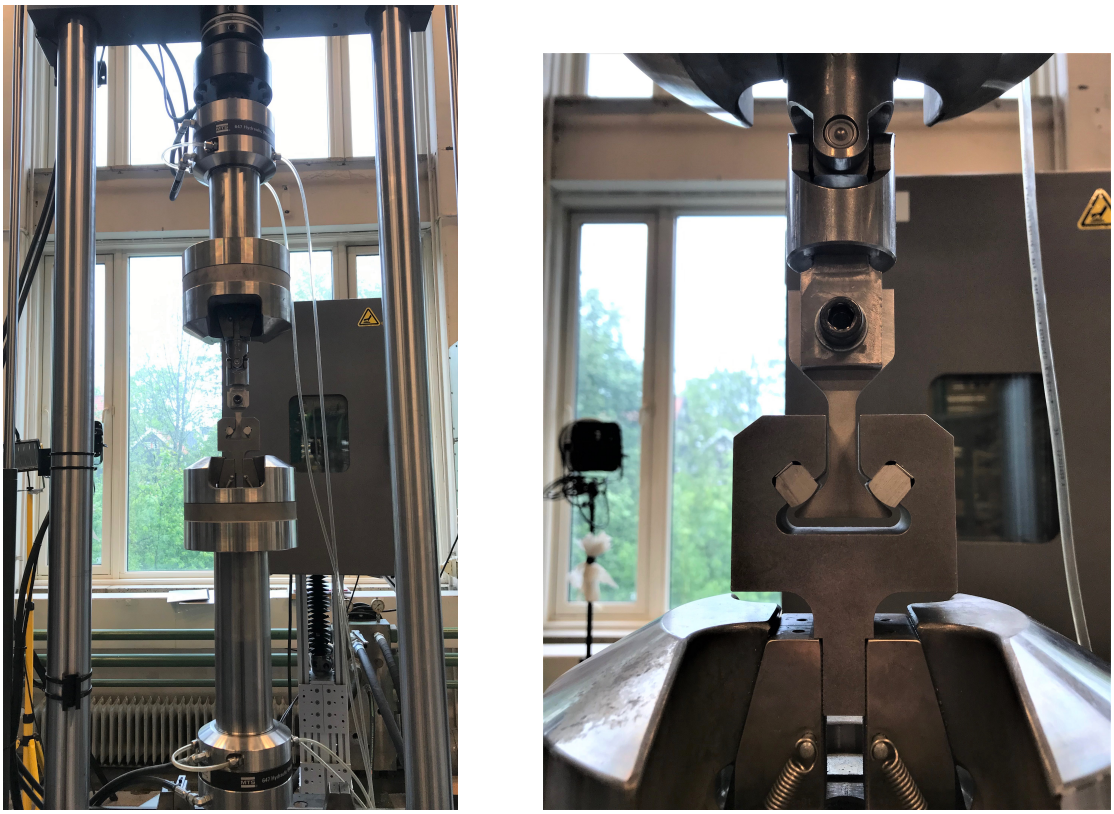

(a) (b)

Figure 28: MTS machine with fretting rig

4.2.1 Fatigue machine

The fretting fatigue testing is performed in room temperature with an MTS Landmark Servohydraulic Test System. The loading frequency is 10 Hz load controlled sinusoidal loading. The test is pure tension, with an R-ratio of 0.1 for all specimens. When testing, a maximum and minimum load is defined.When the test starts the loading is ramped up to the mean load before the cyclic loading begins. It is important to set a good trigger limit to ensure that the machine terminates the test when a crack occurs, the trigger limit is set to 0.85 mm.

The grips clamps the fixture and multiaxial joint with a pressure of 500 MPa. Fig. 28 show the MTS machine with the fretting setup.

Strain gauges are attached at the neck of the specimen to capture the exact moment of crack initiation, and to be able to investigate the crack growth. The strain gauge type is FLAB-3-11-3LJCT-F, with a gauge factor of 2.09 ± 1 and gauge resistance 120 ± 0.5.

The decision regarding load level for testing is typically based on experience. As this is the first test performed with this setup, the first batch will be used as a trial. A maximum load of 5 kN is chosen as origin, the method for choosing the next loading is inspired by the staircase method. The first batch will also give an estimation of the maximum and minimum loads that will lead to fretting failure for Al6082.

5 Numerical Work

This section describes the methodology of the numerical work performed in this thesis, the work is divided into three parts. A study of stick/slip behaviour is presented first, followed by the main study of the dovetail geometry and last an analytic approach to predict fretting failure. The results are presented in Section 6.

5.1 Study of stick/slip behaviour

In the preface for this master thesis, a finite element analysis of fretting fatigue of a dovetail was performed. The results regarding the stick/slip behaviour were not conclusive, giving distinct jumps as illustrated in Fig. 29.

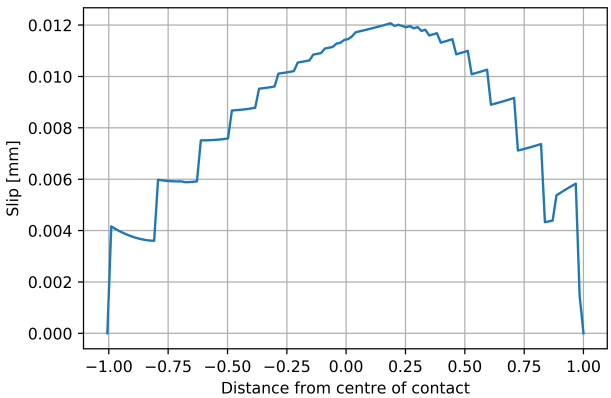

Figure 29: Stick/slip behaviour from dovetail study

As an effort to understand the stick/slip behaviour for the dovetail geometry, a simplified study based on Araújo and Nowells paper from 2002 [4] is performed. The dovetail is simplified from Fig. 30(a) to Fig. 30(b).

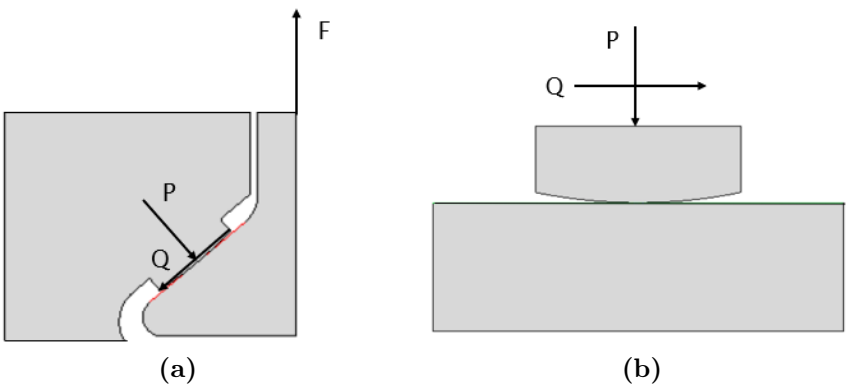

Figure 30: (a) Dovetail geometry with contact loads and (b) simplified approximation

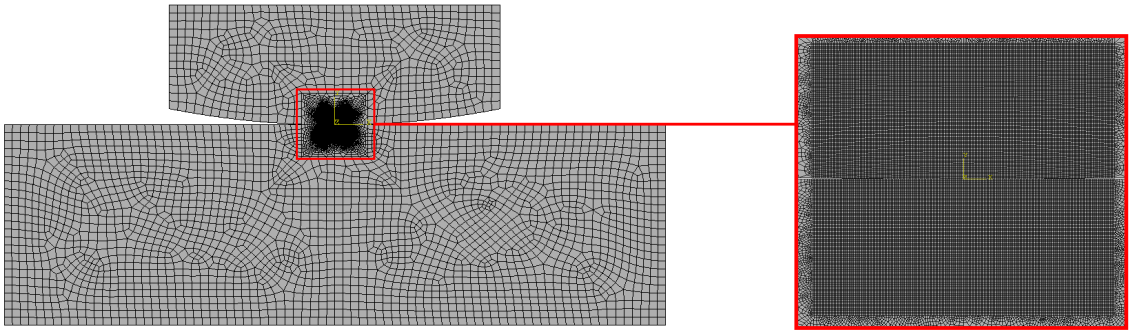

Figure 31: Meshing of model with detail of refined mesh in contact area

The study is performed for two different loading cases, but with the same geometry and material. The material data is listed in Table 2. The friction coefficient is kept at 0.75, and the pad radius is 25 mm in both cases.

Table 2: Material data used in *Abaqus* for stick/slip study

Material	Young's modulus (GPa)	Poisson's ratio	Mass density (kg/m^3)	Yield strength (MPa)
Steel	210	0.3	7800	350

The mesh is illustrated in Fig. 31, with a fine mesh of 5 μm in the contact area and a more coarse global mesh. Due to convergence issues with the *Lagrange multiplier* and to keep the simulation time short, the *penalty method* is used as tangential behaviour.

Case one is the simplification of the dovetail using the geometry in Fig. 30(b). Both the normal pressure (P) and shear force (Q) is applied simultaneously to illustrate the applied load F in Fig. 30(a). The ratio between P and Q gives the angle between the applied load F and the contact surface for the dovetail in Fig. 30(a).

Case two is performed as in the paper by Araújo and Nowell [4], where the normal pressure (P) is first applied, and then the shear force (Q) with the ratio $Q/P = 0.45$.

To control the loading situation, a displacement boundary condition is used in both x- and y-direction. The y-displacement is set to $-0.01mm$, while the x-displacement is varying depending on the wanted angle between Q and P.

5.2 Main FE study

The main study is a FEA of the new test rig at NTNU. To reduce the simulation time, the model is reduced from a full 3D model to a 2D simplification. Fig. 32 show this process. The 2D model is reduced by symmetry to only half the model. When making this reduction, it is important to apply the correct boundary conditions along the symmetry axis. The universal joint is not included in the FE analysis.

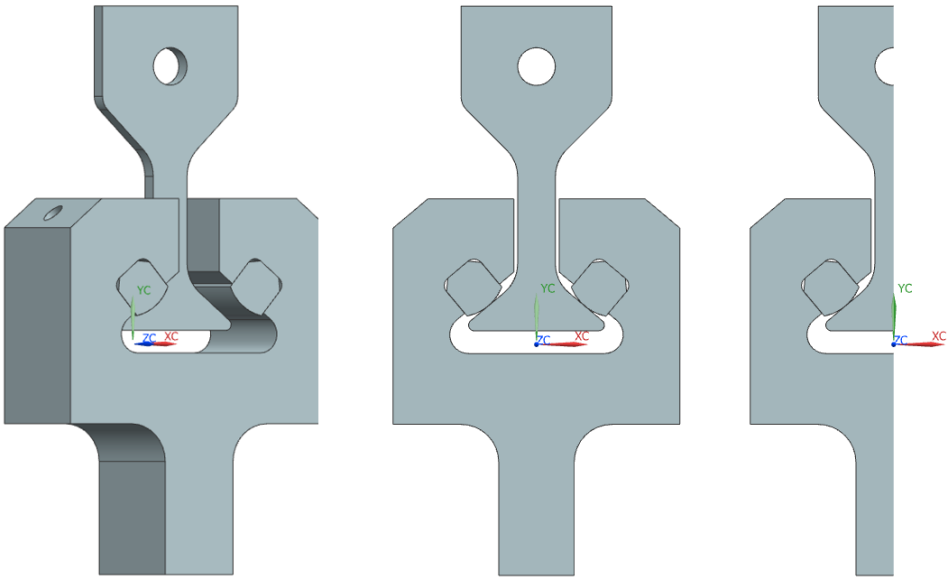

Figure 32: Reduction of the model

In order to obtain correct results in the contact area without a long simulation time, the contact area is partitioned. This allows for a fine mesh in the important areas and a more coarse mesh for the rest of the model. This partition is illustrated in Fig. 33.

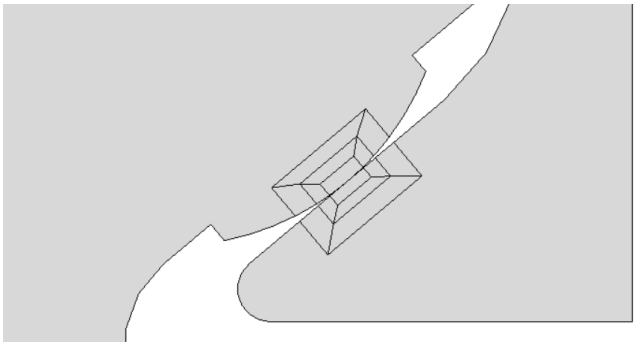

Figure 33: Partition of the contact area

5.2.1 Meshing

The quality of the mesh is of great importance for the FE analysis, and when simulating fretting fatigue the contact area is particularly important. To make sure that the simulation capture the correct stress distribution, a mesh convergence test has been performed. The Lagrange multiplier had fewer convergence problems with this model, than the simplification in Section 5.1, and is therefore used as tangential behaviour. The results are presented in Table 3.

The results display a great difference with the larger elements, but around $0.015mm$ the stresses begin to converge. Interestingly, the model was converged in terms of contact pressure with relatively few elements. With an element size of $0.005mm$ the Lagrange multiplier had convergence problems, and the reported value in the table is from analysis with the penalty method. From the results of the convergence test, an element size of $0.01mm$ in the contact area is found to be sufficient.

Table 3: Mesh convergence test in contact area

Mesh size $[mm]$	Elements in contact	Peak σ/σ_{fine}	Peak p/p_{fine}
0.005	147	1	1
0.01	75	0.98	0.99
0.015	50	0.98	0.99
0.03	24	0.93	0.98
0.05	14	0.89	0.97

The meshing of the model is illustrated in Fig. 34, for specifications see list below.

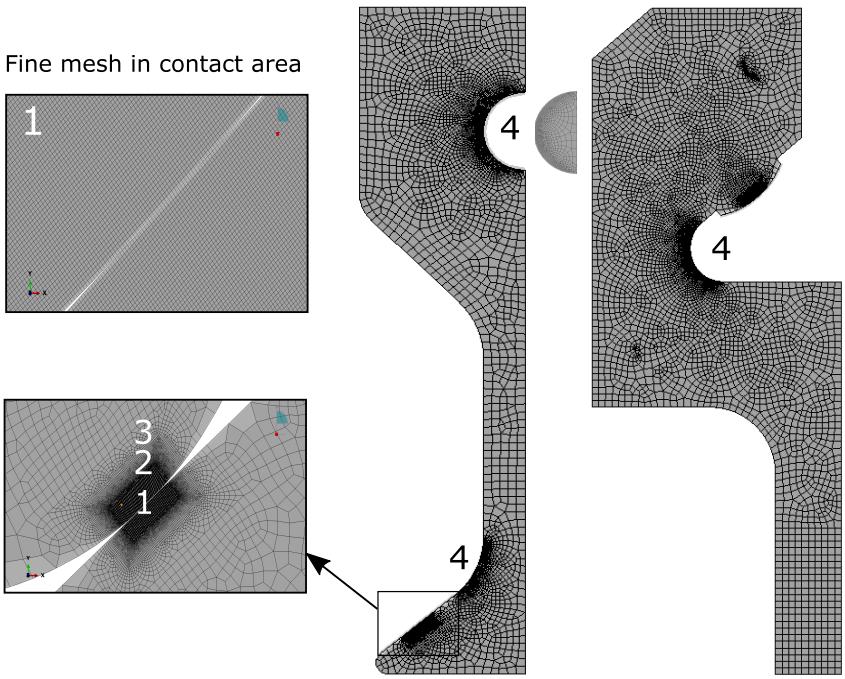

Figure 34: Illustration of mesh

(1) Element size: 0.01 mm

(2) Element size: 0.01-0.05 mm

(3) Element size: 0.05-0.25 mm

(4) Element size: 0.125 mm

For the coarser mesh the element size is set to be 1 mm. The element type used is 4-node plane strain; CPE4R.

5.2.2 Loading and boundary conditions

Because of the symmetry reduction of the model, it is important to apply the correct boundary conditions (BC). The reference points, RP-1 and RP-2, are attached to the model with an equation constraint. This is done to ensure that the model and loading is kept correctly along the y-axis. Fig. 35 show the placement of each boundary condition and the load, an explanation is given in the following list:

- **Load:** the load is attached to RP-2 in the middle of the bolt as a concentrated force. The exact load will vary depending on the simulation, but the R-ratio is 0.1
- **BC-symmetry:** illustrated with blue and orange arrows along the left side of the model. The BC type is symmetry/antisymmetry/encastre, with XSYMM where U1=UR2=UR3=0
- **BC-fixture:** illustrated with orange arrows attached to RP-1 below model. BC type is displacement/rotation and is fixed in the y-direction.

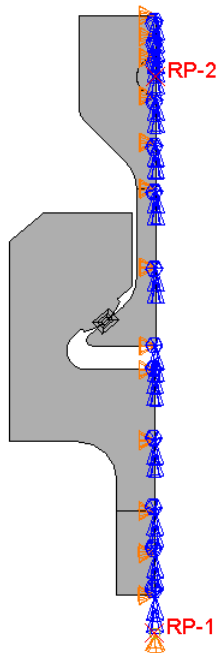

Figure 35: Model with loading and boundary conditions

5.2.3 Interactions/contact formulation

It is important to correctly define the contact between the dovetail and fretting pad to get accurate results. Fig. 36(a) illustrates the surface-to-surface contact between the two bodies, highlighted in red. The master-slave technique is used where the fretting pad is defined as the master surface, and the dovetail is defined as the slave surface. The normal behaviour is set to "*hard contact*" for all analyses, this minimises the penetration of the slave surface into the master surface. When simulating fretting the *Lagrange multiplier* is recommended as tangential behaviour, but the *Penalty* method and *Augmented Lagrange* is also possible choices. Therefore, three simulations with different formulations will be submitted before deciding the appropriate formulation.

The friction is known to be important in fretting, and the COF used in this thesis is based on Araújo and Nowell's [4] measurements for aluminium to aluminium contact. The COF is therefore set to be 0.75.

The contact between the dovetail and the bolt is defined as a surface-to-surface contact, highlighted in blue in Fig. 36(b). This is to ensure that the bolt is kept in place and that no fretting or fatigue failure will occur in this area. The contact formulations are the same as for the contact area, but with COF set to 0.5.

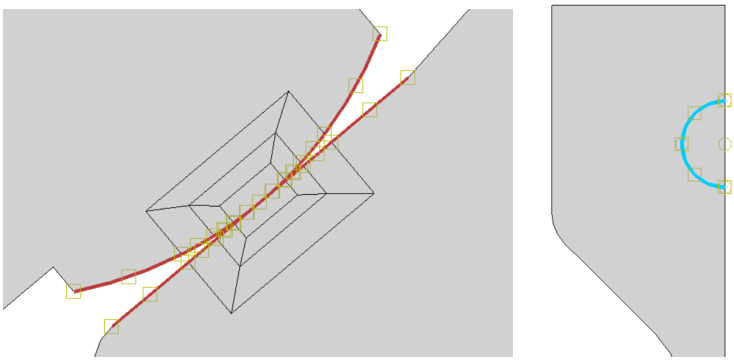

(a) **(b)**

Figure 36: Interactions between dovetail and (a) fretting pad and (b) bolt

5.2.4 Simulations and aim

The simulations will be used to produce contact plots along the path in Fig. 37(a). The analysis is Static General and will be submitted for different loads and contact formulations.

The simulations will be used together with the theory of critical distance. The path is in this case normal to the contact, where the model goes from contact to no contact, illustrated in Fig. 37(b). The exact position for this path will be varying depending on the load, but always situated at the point with the maximum in plane stress.

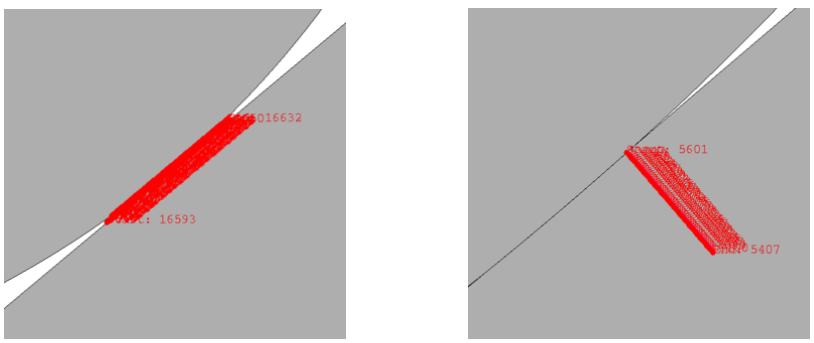

(a) **(b)**

Figure 37: Illustration of path (a) along contact area and (b) normal to the contact area

5.3 Analytic prediction of failure

In order to use TCD, the fatigue limit and threshold need to be known. Normally, these values are obtained from a fatigue test of a plain specimen, but in this case the values are obtained from literature. Atzori et al. [43] have listed different materials together with their fatigue properties. For a similar material, Al 2024, with $R = 0$, they report: $\Delta\sigma_0 = 172MPa$ and $\Delta K_{th} = 4MPa\,m^{1/2}$. This gives a critical length $L = 0.172mm$.

In order to predict failure, the TCD will be used with Sines criterion given by Eq. 23.

$$E_{SI} = \frac{\sqrt{3J_2} + \alpha p_m}{\beta} \tag{23}$$

where J_2 is the second invariant of the stress tensor and p_m is the average hydrostatic stress. These two variables can be extracted directly from Abaqus as Mises and Pressure stress components, respectively. The constants α and β is given by:

$$\alpha = 2\frac{\sigma_{-1}}{\sigma_0} - 1 \tag{24}$$

$$\beta = \sigma_{-1} \tag{25}$$

where σ_{-1} is the fatigue strength for tensile load at $R = -1$, and σ_0 is the fatigue strength at $R = 0$. The fatigue strengths are found from literature [43], and set to $\sigma_{-1} = 248MPa$ and $\sigma_0 = 172MPa$

The exact process to predict failure is illustrated in the flow diagram in Fig. 38. The prediction will only give an assumption on if the specimen will fail or not.

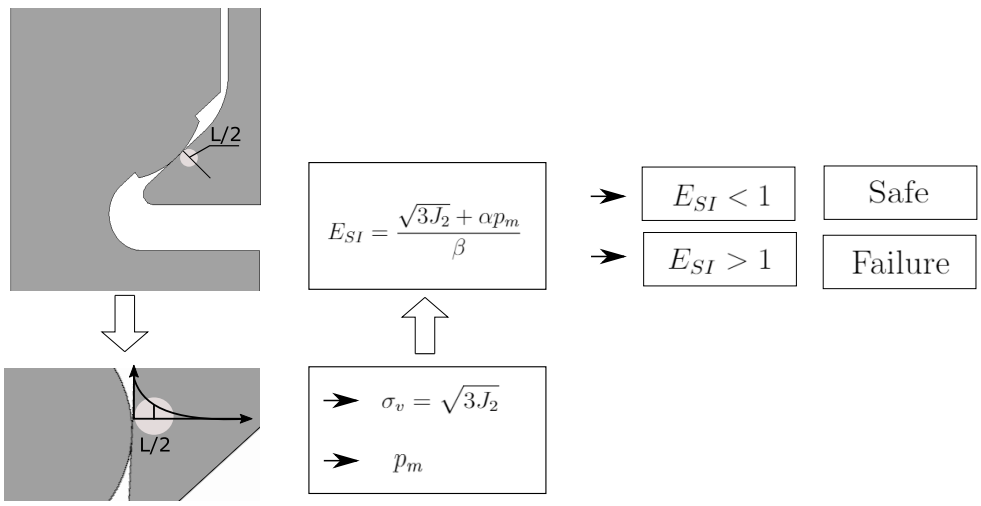

Figure 38: The procedure to apply the Sines criterion in terms of the TCD for fretting fatigue

6 Results

6.1 Experimental results

This section presents the results from fretting fatigue tests of two different batches of Al6082. One produced by CNC, henceforth referred to as batch 1, and one by EDM, referred to as batch 2. Run-out is defined at $2 \cdot 10^6$cycles. The results are classified as fretting or plain fatigue, depending on the location of the crack. All fretting fatigue failures occurred on the trailing edge of contact, while the plain fatigue failure occurred in the notch, this is illustrated in Fig. 39.

(a) **(b)**

Figure 39: Schematic illustration of crack for (a) fretting fatigue and (b) plain fatigue. The contact area is marked grey.

6.1.1 Results Al6082, batch 1

Table 4 lists the results of the tests performed on batch 1. This is the first batch tested with the new test rig, and the main goal is to gather information regarding possible loading intervals and other important factors that influence the result. The pad height is 10 mm for all tests, except specimen no. 8 where it was added 2mm.

The results revealed the importance of new and clean fretting pads for each test-run. Specimen 3 and 4 were tested with used fretting pads leading to plain fatigue failure, for specimen 5 the pads were unused and the surfaces were cleaned with ethanol. This treatment resulted in fretting fatigue instead of plain fatigue failure.

The maximum loading interval is estimated to be in the range of 4 and 7 kN. As this batch was used as a preliminary investigation is it small variations between each test and the results can only be used for guidance.

Table 4: Experimental results from dovetail fretting test, Al6082 batch 1

Specimen no.	R	Frequency [Hz]	F_{max} [N]	F_{min} [N]	N_f	Failure mechanism
1	0.1	10	6000	600	237052	Fretting fatigue
2	0.1	10	5000	500	1050188	Fretting fatigue
3	0.1	10	7000	700	114482	Plain fatigue
4	0.1	10	7000	700	135261	Plain fatigue
5	0.1	10	7000	700	227195	Fretting fatigue
6	0.1	10	5000	500	837682	Fretting fatigue
7	0.1	10	6000	600	384889	Plain fatigue
8 (+2mm)	0.1	10	6000	600	165830	Fretting fatigue

6.1.2 Results Al6082, batch 2

Table 5 lists the results of the tests performed on batch 2. The original pad height was 11mm, but the results from the first two specimens indicated that this was not adequate. It was therefore added additional height to the fretting pads. The added height is noted behind the specimen no. in the table. Specimen 15 is tested three times to provoke fretting fatigue due to limited time.

Table 5: Experimental results from dovetail fretting test, Al6082 batch 2

Specimen no.	R	Frequency [Hz]	F_{max} [N]	F_{min} [N]	N_f	Result
1	0.1	10	5000	500	347543	Plain fatigue
2	0.1	10	4500	450	342967	Plain fatigue
3 (+2mm)	0.1	10	4500	450	619154	Fretting fatigue
4 (+2mm)	0.1	10	4000	400	791348	Plain fatigue
5 (+2mm)	0.1	10	5000	500	483678	Plain fatigue
6 (+4mm)	0.1	10	5000	500	1871232	Fretting fatigue
7 (+2mm)	0.1	10	4500	450	879822	Plain fatigue
8 (+2mm)	0.1	10	4500	450	685381	Fretting fatigue
9 (+2mm)	0.1	10	3500	350	2305047	Run-out
10 (+2mm)	0.1	10	6000	600	266090	Plain fatigue
11 (+2mm)	0.1	10	5000	500	648256	Plain fatigue
12 (+2mm)	0.1	10	4000	400	1041701	Plain fatigue
13 (+2mm)	0.1	10	6000	600	263389	Plain fatigue
14 (+2mm)	0.1	10	6000	600	295153	Fretting fatigue
15* (+2mm)	0.1	10	3500	350	770021	-
15* (+2mm)	0.1	20	3500	350	126672	-
15* (+2mm)	0.1	20	4000	400	4455	Fretting fatigue

* Specimen no. 15 was tested three times

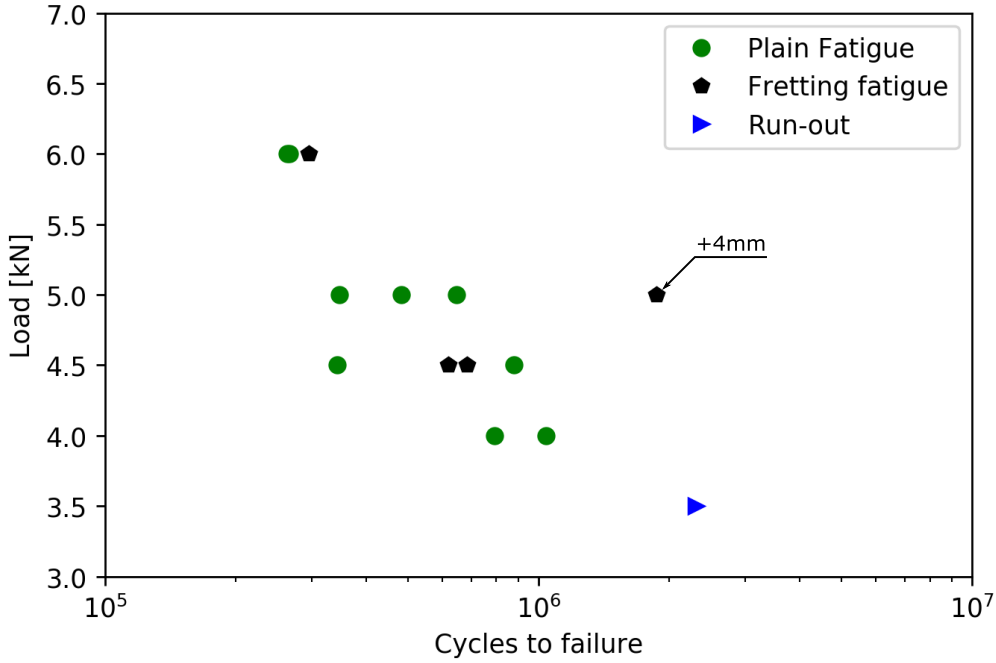

Figure 40: Fatigue data Al6082, batch 2

The results are presented in Fig. 40. Due to small changes through the procedure, it is not possible to draw any trend line through the S-N curve, but it is still possible to see a trend. There are only four data-points for fretting fatigue that can be compared, but they correspond well. The data-point from specimen 6 stands out, this is expected as the pad was 2 mm higher, a contact point closer to the notch gives a smaller moment hence lower bending stress in the notch. There is an amount of scatter for the plain fatigue failure, but it is a clear trend.

6.1.3 Strain gauge data

The failure process is divided into different regimes. The time until crack initiation, and the duration of crack growth leading to failure. It is possible to estimate the time for crack initiation from the strain gauge data.

Batch 1

The strain gauge data presented is from specimen no. 6, which is a CNC-milled dovetail tested with EDM-produced fretting pads. The maximum load is 5 kN and $N_f = 837682$. The data presented is for the last 46000 cycles.

Fig. 41(a) and (b) gives the results from the left and right strain gauge, respectively, and show the last cycles until failure. The graphs show a clear change in displacement before failure occurs, this suggests that the crack initiated some time before the test was terminated. The fracture occurred on the left side, this is represented by the increased change in slope in Fig. 41(a) compared to (b). The results from the strain gauges indicate that the crack initiated more than 46000 cycles before failure, as the slope is changing through the whole time period. This can also be seen from the hysteresis loops in Fig. 41(c) and (d). It is clear that the specimen is in the crack growth regime as the slope is changing for each time-step. The loops indicate partial slip due to the area inside the loop, this is characteristic commonly observed with fretting.

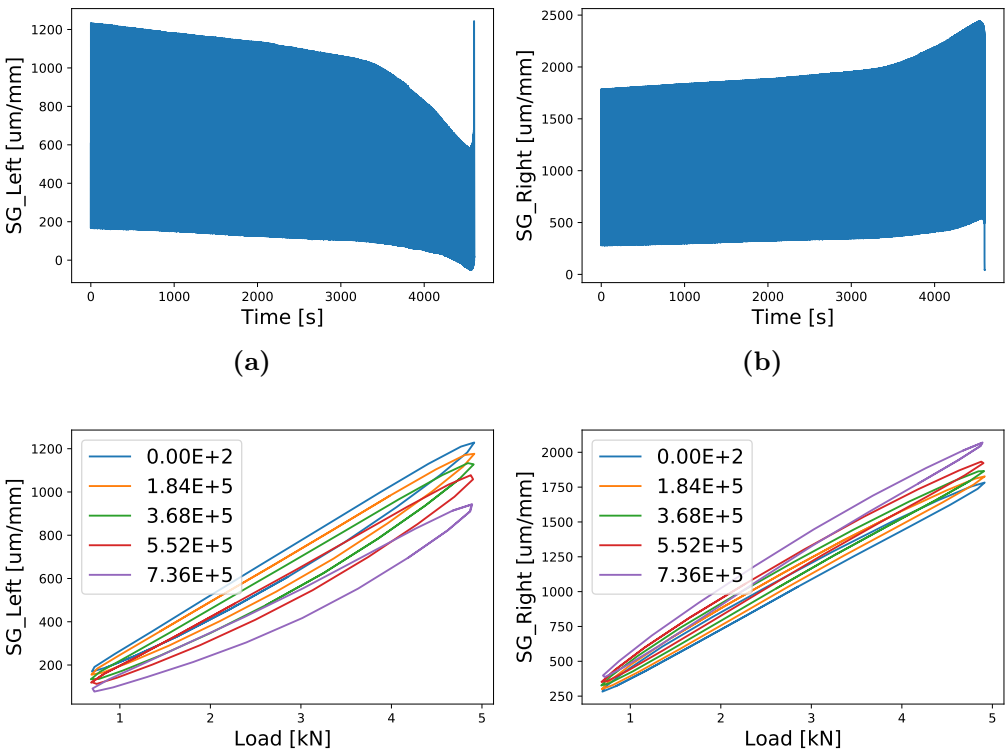

Figure 41: Results from strain gauges for specimen 6, (a) left strain gauge versus time, (b) right strain gauge versus time, (c) left hysteresis loop and (d) right hysteresis loop

Batch 2

Results for the last 51000 cycles for specimen no. 5 are given in Fig. 42. The maximum load is 5 kN and $N_f = 483678$. It is clear that the results are quite similar as in Fig. 41.

From Fig. 42(a) and (b) it can be seen that failure occurred on the left side of the specimen. This is also illustrated in Fig. 44, which is a picture of this particular specimen. The change in the slope is visible for this test as well, but not as distinct as for the specimen in batch 1. From the hysteresis loops in Fig. 42(c) and (d) it is clear that the crack initiated some cycles before the test failed, this is due to the clear change in the slope towards the end. The partial slip is visible for this specimen as well.

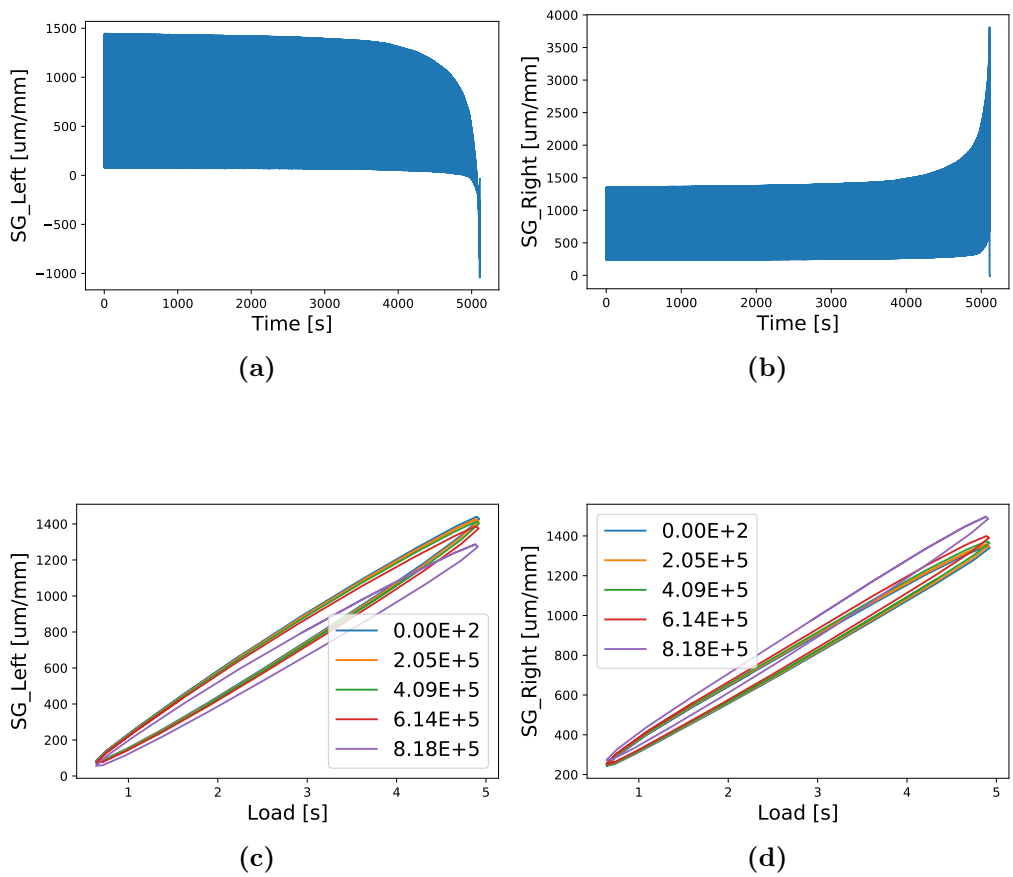

Figure 42: Results from strain gauges, (a) left strain gauge versus time, (b) right strain gauge versus time, (c) left hysteresis loop and (d) right hysteresis loop

By further investigation of the data from the strain gauges, it is possible to find the approximately time for crack initiation, i. e., where the slope changes. From Fig. 43 it can be seen that the slope changes at approximately 2700 s, this is 24000 cycles before failure. Based on this, the crack initiated at approximately 460000 cycles, and the crack growth lasted for about 24000 cycles before the crack was detected by the machine.

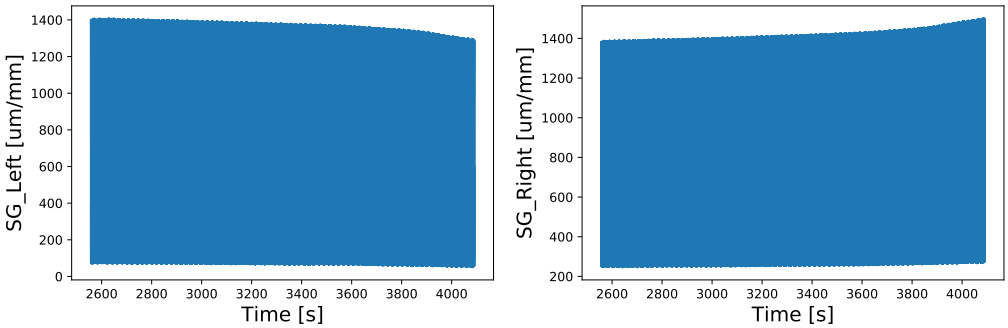

(a) **(b)**

Figure 43: Investigation of crack initiation, strain gauge data from (a) left and (b) right

Figure 44: Failed dovetail in the test machine, specimen no. 5 from batch 2

6.1.4 SEM

The Scanning Electron Microscope (SEM) has been used to characterise the fracture surface, shown in Fig. 45. In Fig. 45(a) one can see striations, marked with red arrows, moving from the edge. This indicates that the crack initiation occurred in the area marked with a red rectangle. Fig. 45(b) and (c) gives more detailed images from this area. The clear wave formations indicate a ductile fracture. The highlighted areas are given in Fig. 45(d) and (e). The formations indicate that the crack initiation occurred in this area. It should be noted that some oxidation from wear on the fretting surface may be present at the edge.

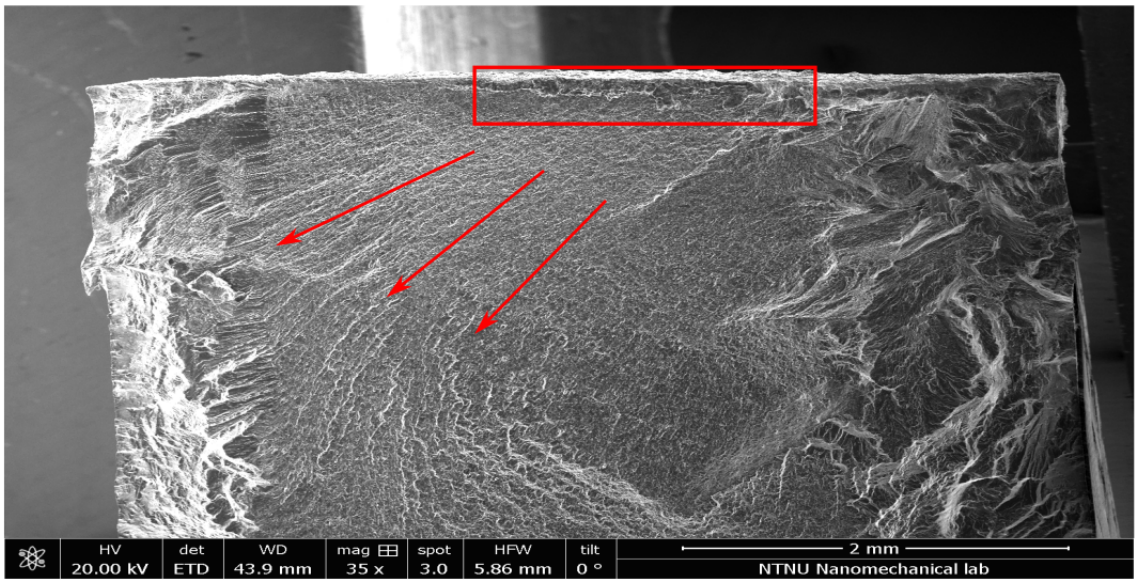

(a)

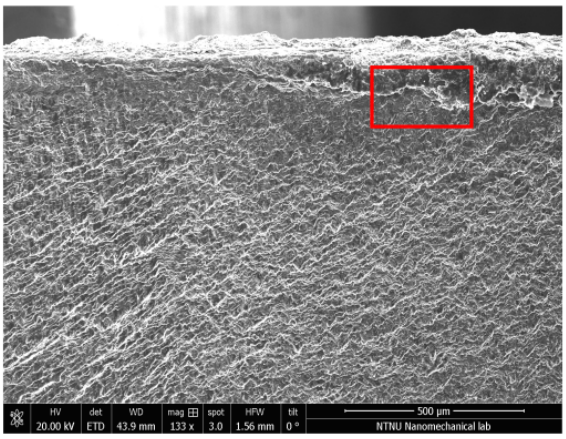

(b)

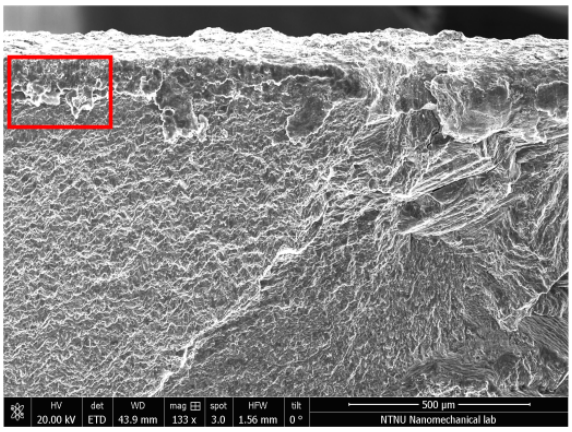

(c)

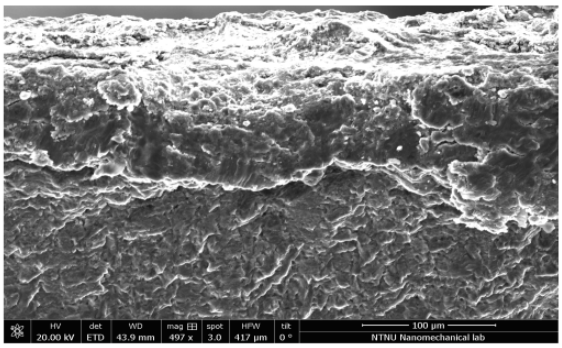

(d)

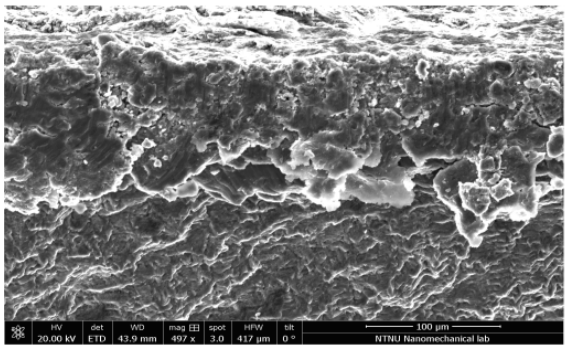

(e)

Figure 45: Fracture surface for dovetail

6.2 Numerical results

This section gives the results from the finite element analysis, for both the stick/slip behaviour and the main study of the dovetail geometry, and the analytic prediction of failure.

6.2.1 Stick/slip behaviour

Fig. 46 shows the von Mises stress distribution for case one and case two, respectively. The peak value of the stress is 574 MPa for case one, and 725 MPa for case two. Thus higher peak value for case two, the stress is high for a larger area in case one.

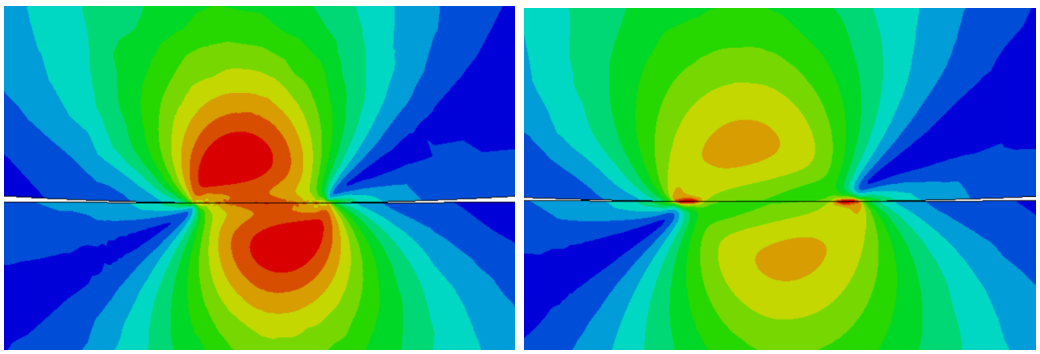

(a) **(b)**

Figure 46: Von Mises stress distribution over contact area for $Q/P = 0.45$ (a) Case one and (b) Case two

Fig. 47(a) and (b) show the stick/slip plot from *Abaqus* for both cases. As expected, the plot for case two, Fig. 47(b), show a clear stick zone in the middle of the contact area, while the edges slip. This is as predicted from the theory regarding Hertzian contact. The results for case one in Fig. 47(a) consists of many small peaks, it is hard to conclude if the two bodies are sticking or slipping over the contact area.

In order to investigate the peaks, the analysis is repeated with additional increments. The plots in Fig. 47(c)-(e) show the stick/slip behaviour for both 10 and 100 increments, and for the two cases $dispX < dispY$ and $dispX > dispY$.

The difference between (c) and (d) is expected as the ratio between Q and P in Fig. 47(d) exceeds the friction coefficient, which gives full sliding between the two bodies, but it is interesting how an increase in increments removes a significant amount of numerical noise. For $Q/P = 0.45$ in Fig. 47(c) 10 increments give fewer peaks, but the peak value is significantly higher. With 100 increments the slip is almost zero, if this is realistic or not is hard to conclude. Fig. 47(e) and (f) show the distribution of von Mises stress in the contact area with 10 and 100 increments respectively. An increase in increments gives a significantly smoother distribution, which is connected to the reduction in numerical noise in the slip curve.

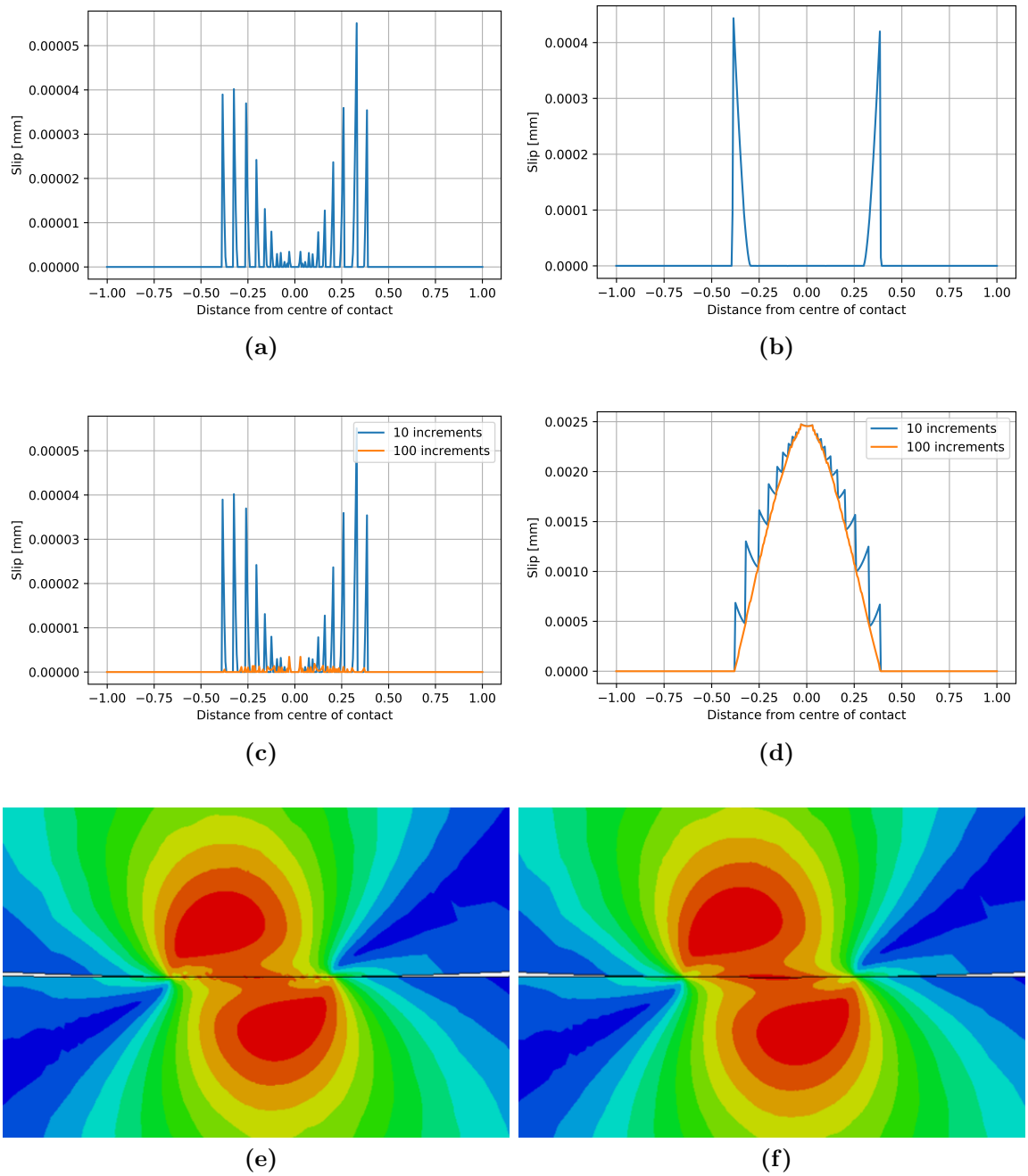

Figure 47: Stick/slip for $Q/P = 0.45$ for (a) Case one and (b) Case two. Stick/slip for (c) $Q/P = 0.45$ and (d) $Q/P = 1.40$, and von Mises stress for (e) 100 increments and (f) 10 increments

6.2.2 Main FE study

This section will show differences between the contact formulations, and give the general contact plots from the FEA of the dovetail. The simulations consist of three steps, pull, release and pull again. This is to simulate a fatigue test. The maximum value of the applied load is $2500N$, and the R-ratio is 0.1.

Contact formulation

The simulations have been performed with three different contact formulations, the penalty method, Lagrange multiplier and augmented Lagrange. Fig. 48 illustrates the stress distribution over the contact area for the three methods. The results correlate very well, despite the difference in increments used. For step one. the penalty method used 16 increments, Lagrange multiplier used 106 and augmented Lagrange used 119. As the Augmented Lagrange requires more increments without any increase in accuracy, the method is rejected.

The *Abaqus* manual states that the stick/slip behaviour is captured more correctly with Lagrange multiplier than with the penalty method. From Section 6.2.1 it is known that an increase in increments for the penalty method gives an increase in accuracy, but also an increase in time. As the recommended contact formulation can be used without any big disadvantages, the Lagrange multiplier is used as contact formulation in this thesis. However, for some simple simulations, where the stick/slip behaviour is out of the scope, the penalty method is found to be satisfying.

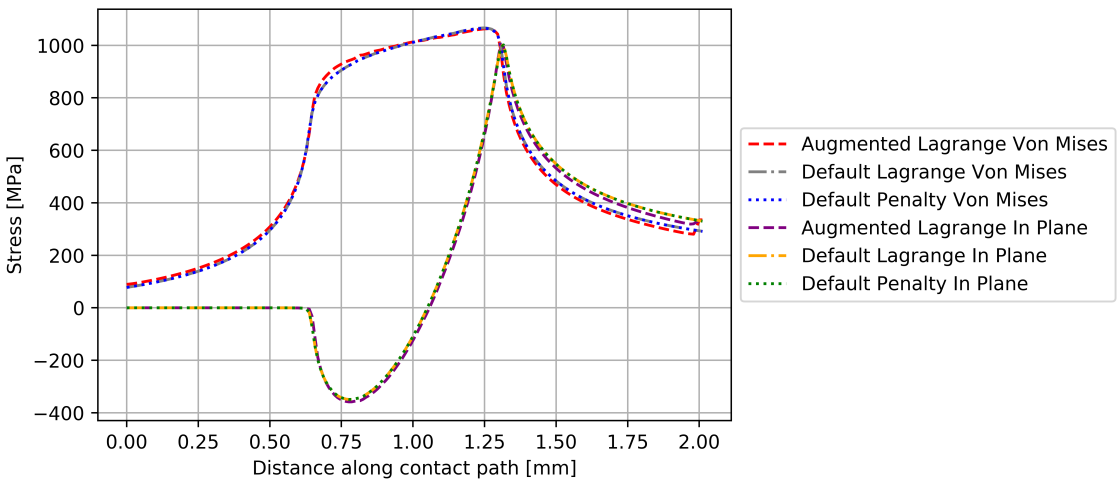

Figure 48: Von Mises and maximum in plane stress distribution over the contact area for different contact formulations

General results

Fig. 49 show the maximum in-plane principal and von Mises stress distribution over the contact area. From Fig. 49(a) one can see a clear stress concentration where the fretting pad and the dovetail go from contact to no contact on the trailing edge. From the literature, it is known that a crack is most likely to occur in this area.

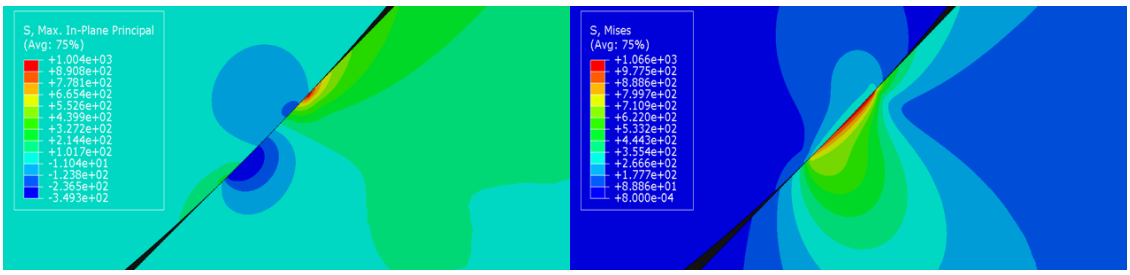

(a) **(b)**

Figure 49: Stress distribution for (a) Max in-plane principal and (b) von Mises

The max in-plane principal and von Mises stress distribution along the contact surface are plotted in Fig. 50(a). The max in-plane principal stress is considered to be the most critical for crack initiation. The stress peaks at both ends of contact, but with opposite direction. The stress concentration at the right side of the contact has a clear peak with about 1000 MPa, this is much higher than the yield-stress for Al6082. This indicates that failure will occur with a load of 5kN for the physical tests. The von Mises stresses are high all over the contact area, but with a peak at the same place as the principal stress.

The contact pressure, frictional shear and slip is plotted in Fig. 50(b) and (c). The plot in Fig. 50(b) is the last increment in step two, i.e., with a loading of 0.1F. Fig. 50(c) is the last increment in step three, where the full load is applied. The slip curve (marked with green) is basically identical for both steps, but the frictional shear and contact pressure differs.

The curve for contact pressure has the same shape but is much slimmer at step two. This is as expected as the load is only 0.1F, and therefore gives a smaller contact area. However, the curve for frictional shear has a completely new shape, the distinct drop in shear stress indicates a stick zone from the centre of contact towards the trailing edge. This zone is visible in step two, and completely gone in step three.

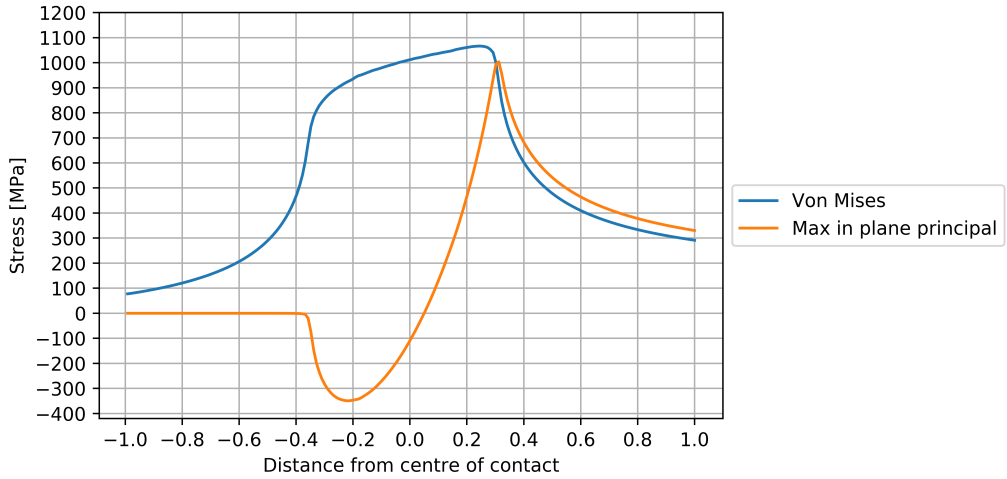

(a)

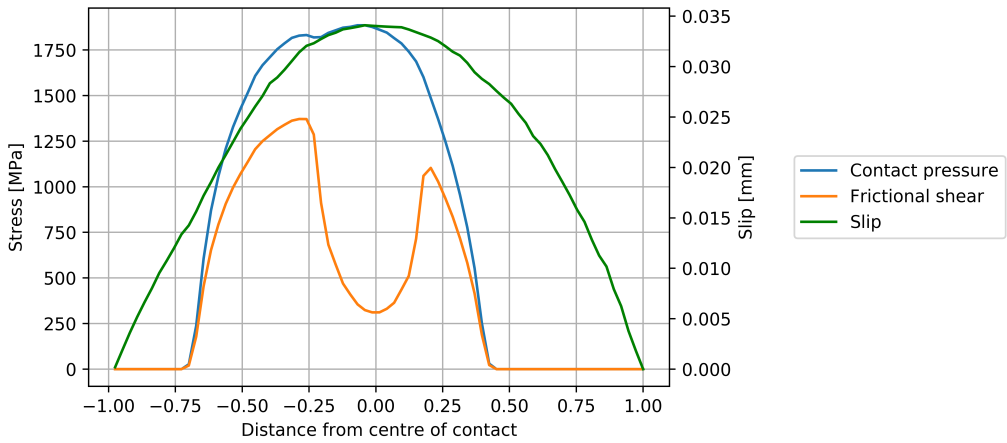

(b)

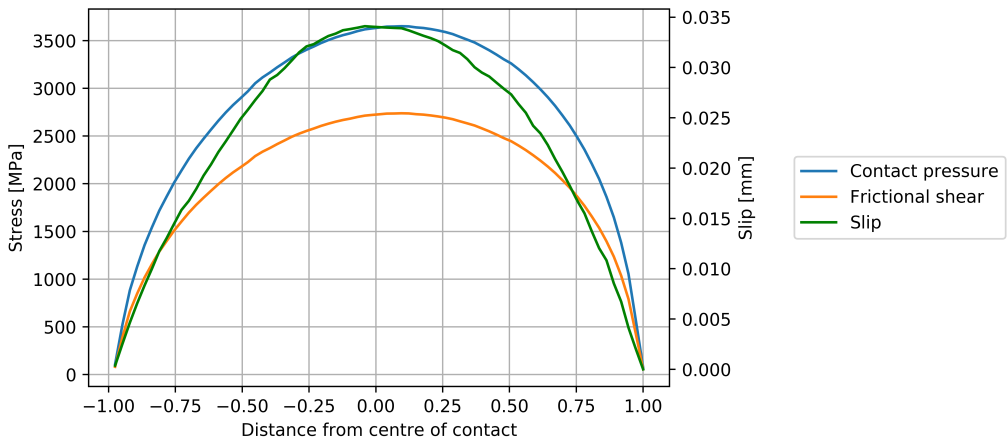

(c)

Figure 50: (a) Max in plane principal and von Mises stress along contact surface. Contact pressure, frictional shear and slip along contact surface for the end of (b) step two and (c) step three

Increasing the load from minimum, $250N$, to maximum, $2500N$, results in the evolution of shear as shown in Fig. 51. The stick zone remains nearly the same size throughout the loading cycle, but decreases drastically to sliding at about 90% of maximum load. When unloading the model back to the minimum load, the shear returns to the same state as at the beginning of the cycle.

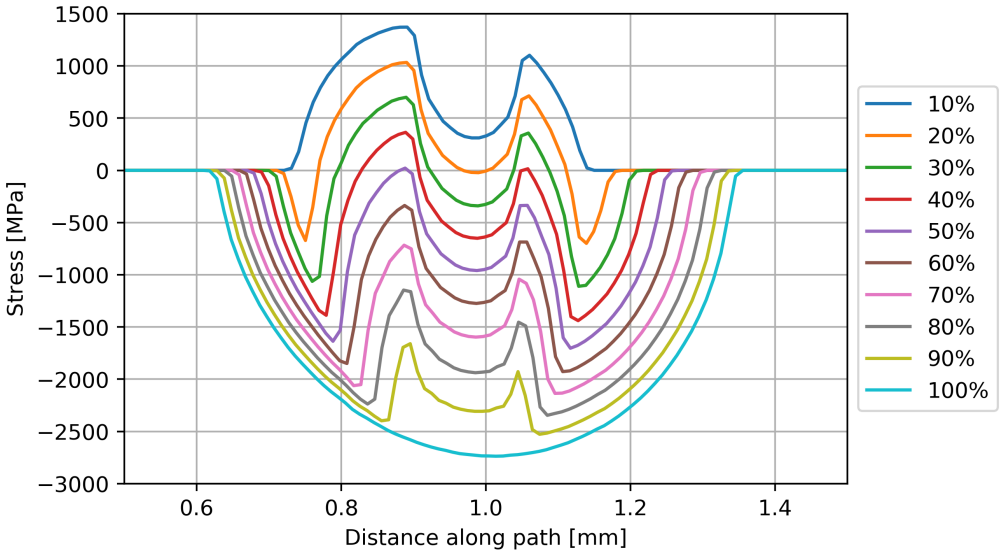

Figure 51: Changes in frictional shear from minimum to maximum load

6.2.3 Analytic results

The analytic prediction of failure is shown in Table 6. The force (F) listed in the table is the maximum applied load in the Abaqus simulation, which is only half of the applied load in physical testing as the model is reduced.

A calculated value for $E_{SI} < 1$ indicate a safe zone where failure do not occur, while $E_{SI} > 1$ indicates failure. Comparing the results whit the physical tests, it is clear that the results correlates well. From the results it can be seen that a limit for the safe zone is slightly above 3 kN.

Table 6: Results from analytic prediction of failure

Specimen no.	F [N]	Avg. Hydrostatic stress [MPa]	Von Mises stress [MPa]	E_{SI}	Result
1	2500	-35.5	387.5	1.5	Failure
1	2000	-17.1	320.4	1.26	Failure
1	1750	-15.3	277.2	1.09	Failure
1	1500	-8.85	234,6	0.93	Safe

7 Discussion

7.1 Test setup

In the initial phase of testing the results turned out to be highly dependent on the environment. The set-up requires high accuracy when placing the specimen as it is important that the fretting pads are equally aligned on both sides. A small misalignment will result in asymmetrical wear, which will influence the results. This misalignment can easily be seen from the fretting scars on the specimens, see Fig 52, where the scar is rectangular for one of the specimens and triangular for the other. It should be noted that the specimens in Fig. 52 are subjected to different loading, respectively a maximum load of $6kN$ for (a) and (c) and $7kN$ for (b) and (d), this is why the scars are more visible on one of the specimens.

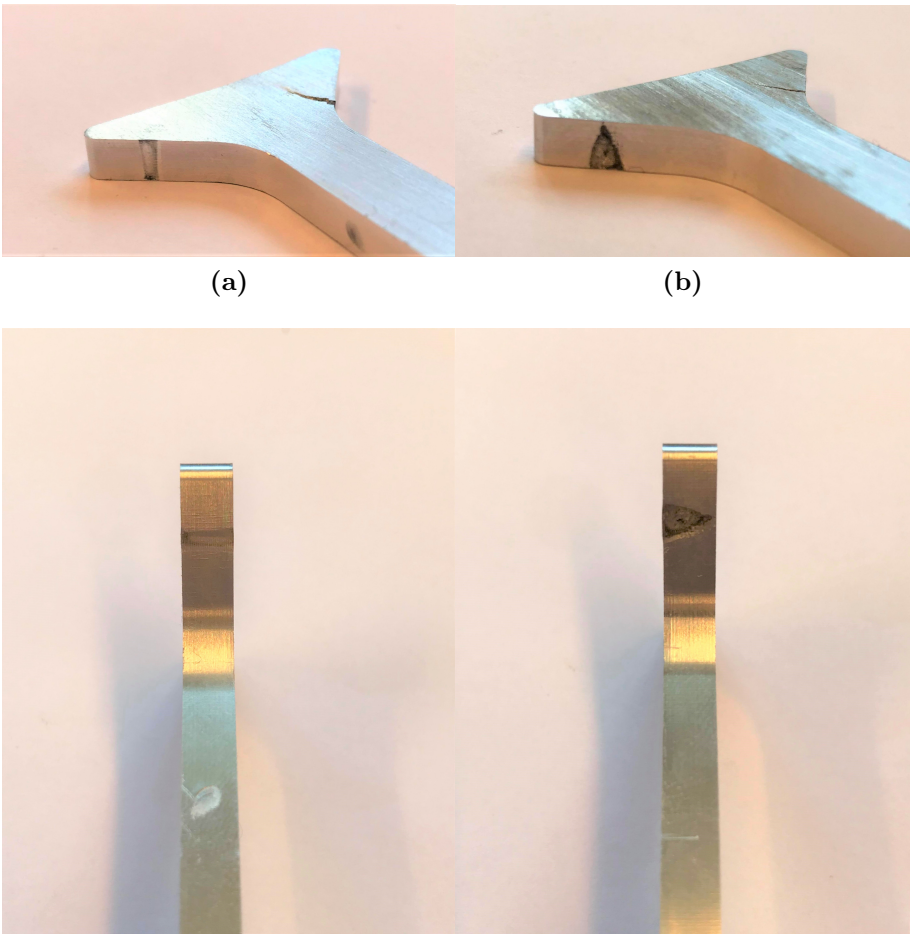

(a) **(b)**

(c) **(d)**

Figure 52: Fretting scars on specimens, (a) and (c) correctly aligned, and (b) and (c) some misalignment

The geometry itself turned out to be fragile. Tests have been carried out with different height (h) on the fretting pads, see Fig. 53. This is to vary the contact

point between the pad and dovetail. The results showed that specimens tested against pads with h=10 mm, i.e., contact point far out on the dovetail, lead to plain fatigue failure in the notch instead of fretting failure the contact area. This may be due to the bending stress created, leading to a stress concentration in the notch. In contrast to this, a high value for h, where the contact is placed high on the dovetail, led to run-outs as it turned out to be hard to provoke fretting fatigue, and most specimens only showed fretting wear. A reason for this may be that the stress created was to low compared to the influenced volume. High contact stresses alone are not enough to provoke inward crack growth, the bulk stress needs to be sufficient to provoke fretting fatigue failure. For situations with lower bulk stress, the dominant failure will be plain fatigue. The increase in pad-height may lead to deformations in the pad, which can change the contact situation in addition to the reduction of bending stress.

The increase in life due to higher pads can be seen in the results for batch two. Specimen 5, 6 and 11 were tested with a maximum load of $5kN$. Specimen 6 with $h = 15mm$, and 5 and 11 with $h = 13mm$. Specimen 6 failed at $N_f = 1871232$ cycles, while specimen 5 and 10 failed at $N_f = 483678$ and $N_f = 648256$ cycles respectively. The increase in life for specimen 6 is with more than 10^6 cycles, which is significant.

The correct value for this height may also be dependent on the material and sample preparation. For the CNC-milled specimens a height of $10mm$ worked quite well, and 11 mm even better. The EDM-produced specimens needed at least 11 mm, preferably 13 mm or more for fretting fatigue to be the dominant failure mechanism.

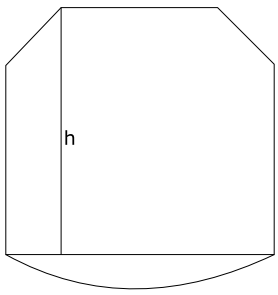

Figure 53: Illustration of the definition of pad height

Fretting is known to be highly dependent on friction, and to limit the scatter in the results it is important that all tests have the same coefficient of friction. In practice this is difficult. It is important to clean both the specimen and fretting pads with ethanol before testing to ensure dry contact with no remains of oil or grease. New fretting-pads should be used for each test. This is to ensure that the contact geometry is kept constant for all specimens. A used pad will have changes in both hardness and roughness.

It is interesting to study both crack initiation and growth, but to capture the exact time of initiation is the most important. A carefully chosen trigger limit was set to the displacement in the fatigue machine to ensure that the machine stops as soon

as possible after initiation, this is to prevent further loading from destroying the initiation area. In contrast, the limit has to be high enough to be able to handle possible elongation of the specimen. For some of the test-runs, the machine did not stop soon enough, leading to a crushed specimen or a long crack. This may result in extra scatter in the S-N curve as the number of cycles to failure may be reported to high. It is possible to extract a more correct number of cycles to failure from the strain gauges data, but this is of course also only an estimation.

As this is the first test-run performed by this test rig, some improvements should be performed. The neck on the specimen should be wider, leading to possibilities for a smoother transition through the notch. This will decrease the stress concentration in the notch, making fretting the dominant mechanism of failure. To enable for this improvement, the opening in the fixture has to be wider as well. A restriction in the set-up is the stiffness in the lower fixture, if the applied load gets big it is possible that the fixture will bend outwards. This will lead to a change in the contact forces. This is negligible at low load levels and for soft materials such as aluminium, but can be an issue with stronger materials. There are also some challenges regarding the correct trigger limit and how to capture the crack initiation. A possibility is to use Digital Image Correlation (DIC) to investigate the process, this can provide a good picture of both crack initiation and growth. Another option is to program the trigger limit to detect a percentage increase in displacement over the last x cycles.

7.2 Scatter in fatigue data

The fatigue data showed some scatter. Fatigue is a "weakest link" failure mechanism, and even a small defect in the material will have a significant impact on the results. This has been proven in this experiment, especially because fretting is even stronger influenced by small defects. As mentioned, a small misalignment when placing the test specimen in the fatigue machine can lead to a major change in fatigue life.

The term "life" is arbitrary, and should be precisely defined. Some define crack initiation as the time when a crack is visible by eye, while some use a crack length of $1mm$ as a limit. The crack length for the failed specimen in this test is varying, this can lead to an overestimation for cycles to failure for some of the tests. E.g., the strain gauge data from EDM-specimen no. 5, showed that crack initiation appears to be approximately 24000 cycles earlier than the reported life. The life could have been adjusted based on the strain gauge data, but this is not performed as the adjustment would have been performed based on speculations. Another reason is that the trigger limit has been the same for all specimens which means that the results are obtained on the same premise.

There are small changes in the different test-runs, and the results can not be directly compared, but it is possible to see a certain trend in the results.

7.3 Sample preparation

The dovetail specimens are made from rolled plates. This may lead to elongated grains, which can influence the fretting behaviour. This could be improved by heat treatment, but the geometry is considered the most critical parameter, and the improvement is therefore not performed. The microstructure may be different for the two batches as well, the rolling direction is not necessarily the same, and this will give different grains

When using EDM it is common that micro-cracks occur on the surface. These cracks are not visible by eye but can be seen in a microscope. Through the fretting process, the contact surface is affected by wear, and the micro-cracks will disappear due to "polishing" in this area. When this happens, the most critical area can be moved to the notch, resulting in plain fatigue failure. To avoid this particular failure, the height of the fretting pads has been increased by adding 2 mm thick shreds. As discussed earlier, this results in a contact area closer to the notch, which decreases the bending stress in this area. Another improvement could have been to polish the surface in the notch before testing to remove possible micro-cracks.

It is reported that EDM-produced components have an increased surface hardness [40]. This increased hardness leads to longer resistance against wear of the oxide layer in the contact area, which is the first stage in the fretting process. The effect of increased hardness could cause defects in the surface to have a more significant impact, leading the material to be less prone to fretting fatigue.

The difference in friction for the two batches can be seen in the hysteresis loops in Fig. 41 and 42. The hysteresis loops for the EDM-produced specimen is slimmer than the loop for the CNC-milled specimen. This correlates well with theory [21], it is known that the hysteresis loop gets slimmer with an increase of friction.

The results from the testing show a clear difference in life between the specimens produced by EDM and CNC. The CNC-milled specimen loaded with 5 kN failed at 1050000 cycles, while the EDM specimens at 5 kN failed between 480000 and 650000 cycles. There is some variation between the test procedure for the two batches, and the results can not be directly compared. Nevertheless, the results indicate a significant decrease in life for the EDM produced specimens.

7.4 FEA results

In the *Abaqus* user manual [38], it is stated that the Lagrange multiplier is recommended for fretting simulations. Several tests have been submitted with the penalty method, Lagrange multiplier and augmented Lagrange as contact formulation. The differences are small between all analyses; the stress distributions, contact pressure and frictional shear are approximately the same. Some differences in the slip curves are visible, i.e., less scatter on the curve with Lagrange. The simulation time is shorter for the penalty method, but it is not decisive. For the analyses with a very fine mesh (5 μm) the Lagrange multiplier had convergence

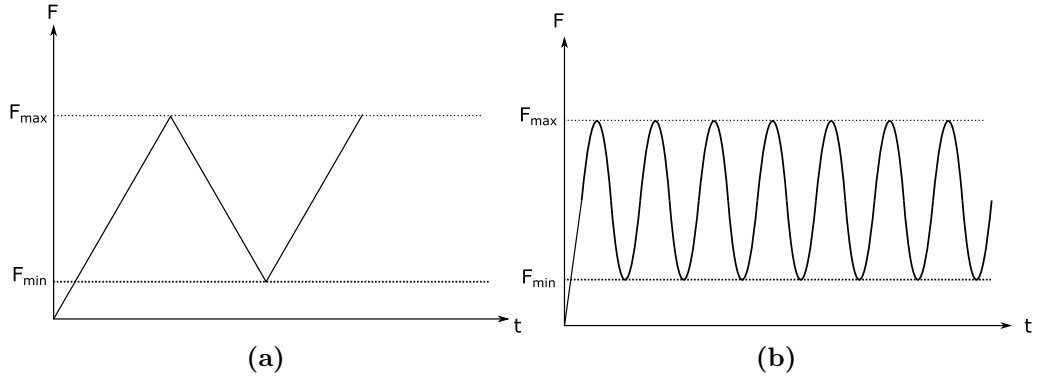

Figure 54: Illustration of loading in (a) *Abaqus* and (b) physical fatigue testing

problems, while the penalty method only used a few more increments in total. It should also be noted that some convergence problems may occur for the Lagrange multiplier if the two contacting surfaces have a considerable difference in stiffness, e.g., steel and aluminium. Comparing all results, it is hard to give general advice on which method that gives the most accurate result, but as it was possible to use the Lagrange multiplier without a substantial increase in time this method was chosen in this thesis. For other cases where the stick/slip behaviour is out of scope, the penalty method with a sufficient number of increments can be recommended to avoid possible convergence problems.

In the *Abaqus* simulations, the load is applied linearly in three steps as illustrated in Fig. 54(a). The load is applied from 0N to F_{max}, down to $0.1F_{max}$ and back to F_{max}. In physical testing, the load is applied in magnitudes of cycles with a sinus curve, as illustrated in Fig. 54(b). In this case, the influence of the first cycle from 0 to F_{max} is negligible, while the ramp in the Abaqus simulation may influence the results. To get confidence in the results, some simulations with five steps have been performed. The results at step two and three were the same as for step four and five. Based on this one can argue that the model with only three steps is sufficient. Note that the linear loading condition in Abaqus is a simplification as contact problems are highly nonlinear and path dependent.

To measure and obtain the correct COF for fretting can be hard [4, 44, 45]. The COF in these simulations is obtained from the calculations for fretting on aluminium to aluminium performed by J.A. Araújo and D. Nowell [4]. This estimation is assumed to be sufficient despite the fact that there are some differences in the alloy.

The COF is most likely changing due to wear and debris during the fretting process, giving a higher COF in the last part of the process. This is not included in the simulations submitted in this thesis and is, therefore, a source of error regarding the reported results. This simplification is not considered to be critical as the aim is to investigate the stress and pressure distribution, not to predict the size of the fretting scars accurately or to predict the exact number of cycles to failure.

Even though there have been performed an individual study regarding the stick/slip behaviour, it is hard to conclude on the exact behaviour. *Abaqus* captures the stick

zone for the dogbone study based on Araújo and Nowell [4], but seems to have problems when the normal and tangential loads are applied simultaneously. In the main study of the dovetail, a stick zone is visible on the shear plot (Fig. 50(b)), while the stick/slip plot is unclear. When the shear is plotted for a whole time-step, the stick zone is visible until the last increment (Fig. 51). Conner and Nicholas [46] experienced the same behaviour in their FE model. They argue that the sliding upon the maximum load is unlikely to be physical as the tangential load will reverse in direction as the load will be reduced when reaching 100%. They conclude that this may be a weakness in the FE model.

The fretting process has been analysed by the FE method for both simple Hertzian contact and the dovetail set-up for a long time. For the studies on Hertzian contact where the normal load P is applied first, and then the tangential load Q, often referred to as Cattaneo-Mindlin, the stick/slip behaviour is studied and explained. E.g., the studies performed by Araújo and Nowell [4], Yue and Wahab [22] and Pereira et al. [47]. In the papers where both P and Q are applied simultaneously, typically in dovetail studies as the ones performed by Rajasekaran and Nowell [41], Conner and Nicholas [46] and Golden [28] the stick/slip behaviour is only mentioned briefly. To the best of the authors knowledge, a complete study of the stick/slip behaviour of the dovetail geometry is not performed, this is uncharted territory in the dovetail study.

7.5 Analytic results

The analytic results only predict if the applied load will lead to failure or not. Comparing the results from the analytic prediction in Table 6 and the experimental results in Table 5 it can be seen that the fatigue limit is at approximately the same loading level, which is slightly above 3kN.

To obtain a more accurate result from TCD the fatigue limit should have been found through a plain fatigue test on a specimen made from the same batch, this was not performed due to limited time and resources. To the authors knowledge, there are no publications regarding fatigue limit and critical distance for Al6082 at $R = 0.1$. Thus, constants used in this thesis are obtained from the study by Azori et al. [43] for a similar aluminium alloy. This simplification is found to be sufficient based on the fact that Araújo et al. used the same source for their assumptions, and that material used in their paper is approximately the same as in this study.

The values used in this report are for $R = 0$, even though the tests performed in this study are at $R = 0.1$. It should be noted that the R-ratio is for the applied load, but it is possible that the R-ratio is different for the contact stresses as contact is nonlinear. As the material constants used are for another alloy, the difference in R-ratio is argued to be negligible. The results are therefore only a simplification but turned out to be a good fit.

The numerical prediction could also use critical plane approaches such as Fatemi-Socie and Smith-Watson-Topper. This could improve the results, but are

time-consuming and therefore not performed. Fretting fatigue is not proportional which makes critical plane approaches essential. This should be investigated in further work.

It is also interesting to use the strain energy density criterion to predict fretting fatigue failure, but this requires a big effort. The location of the critical radius is of great importance. While this placement in the centre of a sharp crack, it is not as straight forward for fretting. The location of the crack is changing depending on the applied load as the contact area gets wider with a higher load. One of the big advantages with SED is that the mesh can be coarse, this is particularly attractive when applying the criterion to fretting where the FEA requires a very fine mesh. From the calculated critical distance in this thesis and Eq. 19, the critical radius R_c is calculated to be $0.13mm$. This seems to be a good fit as theory reports a radius of 0.12 mm for aluminium [17].

8 Conclusion

The main goal for this thesis was to have a working test rig at NTNU. The test setup is working, but still has potential for improvements. The results show a significant difference in fretting failure for the two batches tested in this project, this underlines the complexity when testing fretting failure. The results show a decrease in life for the specimens produced by EDM compared to the traditionally CNC-milled specimens. However, there is not a sufficient amount of results to put a number to this reduction.

There have been performed analyses with both penalty and Lagrange multiplier as tangential behaviour. Even though the Abaqus manual states that the Lagrange multiplier should be used for fretting, the simulations performed in this thesis showed that the penalty method might be as accurate many situations.

The results from the finite element analyses correspond very well with the theory regarding location of the crack, the stress concentration is at the trailing edge of the contact. There has been progress towards the understanding of the stick zone. Studying the frictional shear along contact revealed a possible stick zone in the middle of the contact. The plots regarding the stick-slip are still not conclusive and do not correspond to this stick zone. Based on the results, it is not possible to make any concluding remarks regarding this behaviour, and further research is necessary.

Analytic prediction of fretting failure has been performed. The application of the theory of critical distance combined with Sines criterion gave a sufficient prediction on whether the test would lead to failure or not. Further work should include a combination of TCD and critical plane theories, and it should be possible to give an estimation of life based on this.

9 Further Work

Fretting fatigue is a widespread problem, and the research is still ongoing. Several aspects regarding fretting fatigue are interesting for further research, some will be listed in this section.

- Some adjustment to the test rig should be performed. The neck of the specimen should be wider, enabling for a smoother transition through the notch. This should decrease the number of plain fatigue failures, and increase the probability for fretting fatigue. This improvement will probably also allow for higher applied loads.
- It is interesting to examine the microstructure. A sample have been prepared, only missing the etching process. The examination is not performed due to limited time, but should be included in further work.
- Further investigation regarding semi-analytic and analytic prediction of fretting. Some research on the theory of critical distance and critical plane have been performed, and the results are looking promising but further research is necessary. As the loading is non-proportional, critical plane methods should be used. This can be done in combination with theory of critical distance (TCD). Applying the strain energy density criterion on fretting is another interesting approach. In engineering application, SED is an interesting approach as the mesh do not have to be refined. To the authors knowledge, this is still not performed and therefore a very interesting way forward.
- Further research on the stick/slip behaviour should be performed, both in *Abaqus* and physical testing. The simulations seems to give good results regarding stress, pressure and frictional shear distributions, but the stick/slip behaviour is still not conclusive. It is also interesting to capture the stick/slip behaviour in physical testing, this can be done by Digital Image Correlation (DIC).
- There have been several studies on fretting fatigue in orthopaedic implants, and some estimates that fretting fatigue is responsible for 74% of failures in implants [48]. Additive manufactured titanium is a suitable material for implants, and for these reasons it is interesting to perform fretting fatigue studies on this material. When testing for implants, it is especially interesting to perform tests in fluids as the body fluids are known to be highly corrosive [42]. With the test rig at NTNU this can be done by applying end caps to the lower fixture.

References

[1] D. Nowell, D. Dini, and D. A. Hills. "Recent developments in the understanding of fretting fatigue". In: *Engineering Fracture Mechanics* 73.2 (2006), pp. 207–222. ISSN: 00137944. DOI: 10.1016/j.engfracmech.2005.01.013.

[2] D. Hills and D. Nowell. *Mechanics of Fretting Fatigue*. Solid Mechanics and Its Applications. Springer Netherlands, 1994. ISBN: 9780792328667.

[3] D. A. Hills and D. Nowell. "Mechanics of fretting fatigue — Oxford's contribution". In: *Tribology International* 76 (2014), pp. 1–5. ISSN: 0301679X. DOI: 10.1016/j.triboint.2013.09.015.

[4] J. Araújo and D. Nowell. "The effect of rapidly varying contact stress fields on fretting fatigue". In: *International Journal of Fatigue* 24.7 (2002), pp. 763–775. ISSN: 0142-1123. DOI: https://doi.org/10.1016/S0142-1123(01)00191-8.

[5] N. E. Dowling. *Mechanical Behavior of Materials*. Pearson Education Limited, 2013. ISBN: 9780131395060.

[6] P. P. Milella. "Factors That Affect S-N Fatigue Curves". In: *Fatigue and Corrosion in Metals*. Milano: Springer Milan, 2013, pp. 109–191. ISBN: 978-88-470-2336-9. DOI: 10.1007/978-88-470-2336-9_3.

[7] R. Pollak, A. Palazotto, and T. Nicholas. "A simulation-based investigation of the staircase method for fatigue strength testing". In: *Mechanics of Materials* 38.12 (2006), pp. 1170–1181. ISSN: 0167-6636. DOI: https://doi.org/10.1016/j.mechmat.2005.12.005.

[8] J. Collins. *Failure of materials in mechanical design — analysis, prediction, prevention (2nd ed.)* John Wiley and Sons, Inc, New York, 1993. ISBN: 9780471558910.

[9] E. Gdoutos. *Fracture Mechanics: An Introduction*. Springer, 2005. ISBN: 1-4020-2863-6.

[10] T. Anderson. *Fracture Mechanics: Fundamentals and Applications*. CRC Press, 2017. ISBN: 978-1-4987-2813-3.

[11] A. Giannakopoulos, T. Lindley, and S. Suresh. "Aspects of equivalence between contact mechanics and fracture mechanics: theoretical connections and a life-prediction methodology for fretting-fatigue". In: *Acta Materialia* 46.9 (1998), pp. 2955–2968. ISSN: 1359-6454. DOI: http://dx.doi.org/10.1016/S1359-6454(98)00011-1.

[12] D. Taylor. *The Theory of Critical Distance (1st ed.)* Elsevier Science, 2007. ISBN: 9780080444789.

[13] D. Taylor, S. Kasiri, and E. Brazel. "The theory of critical distances applied to problems in fracture and fatigue of bone". In: *Atti del XX Convegno Nazionale del Gruppo Italiano Frattura* (2009), p. 11.

[14] D. Radaj and M. Vormwald. *Advanced Methods of Fatigue Assessment*. Springer, 2013. ISBN: 9783642307393. DOI: https://doi.org/10.1007/978-3-642-30740-9.

[15] P. Lazzarin and R. Zambardi. "A finite-volume-energy based approach to predict the static and fatigue behavior of components with sharp V-shaped

notches". In: *International Journal of Fracture* 112.3 (2001), pp. 275–298. ISSN: 1573-2673. DOI: 10.1023/A:1013595930617.

[16] F. Berto and P. Lazzarin. "A review of the volume-based strain energy density approach applied to V-notches and welded structures". In: *Theoretical and Applied Fracture Mechanics* 52.3 (2009), pp. 183–194. ISSN: 0167-8442. DOI: https://doi.org/10.1016/j.tafmec.2009.10.001.

[17] P. Livieri and P. Lazzarin. "Fatigue strength of steel and aluminium welded joints based on generalised stress intensity factors and local strain energy values". In: *International Journal of Fracture* (2005). ISSN: 1573-2673. DOI: 10.1007/s10704-005-4043-3.

[18] M. E. M. Eden, M. W. N. Rose, and M. P. L. Cunningham. "The Endurance of Metals: Experiments on Rotating Beams at University College, London". In: *Proceedings of the Institution of Mechanical Engineers* 81.1 (1911), pp. 839–974. DOI: 10.1243/PIME_PROC_1911_081_017_02.

[19] M. P. Szolwinski and T. N. Farris. "Mechanics of fretting fatigue crack formation". In: *Wear* 198.1 (1996), pp. 93–107. ISSN: 0043-1648.

[20] O. Vingsbo and S. Söderberg. "On fretting maps". In: *Wear* 126.2 (1988), pp. 131–147. ISSN: 0043-1648. DOI: https://doi.org/10.1016/0043-1648(88)90134-2.

[21] S. Fouvry, P. Kapsa, and L. Vincent. "Quantification of fretting damage". In: *Wear* 200.1 (1996), pp. 186–205. ISSN: 0043-1648. DOI: https://doi.org/10.1016/S0043-1648(96)07306-1.

[22] T. Yue and M. A. Wahab. "Finite element analysis of stress singularity in partial slip and gross sliding regimes in fretting wear". In: *Wear* 321 (2014), pp. 53–63. ISSN: 0043-1648. DOI: https://doi.org/10.1016/j.wear.2014.09.008.

[23] D. Hills, D. Nowell, and J. O'Connor. "On the mechanics of fretting fatigue". In: *Wear* 125.1 (1988), pp. 129–146. ISSN: 0043-1648. DOI: https://doi.org/10.1016/0043-1648(88)90198-6.

[24] N. P. Suh and H.-C. Sin. "The genesis of friction". In: *Wear* 69.1 (1981), pp. 91–114. ISSN: 0043-1648. DOI: https://doi.org/10.1016/0043-1648(81)90315-X.

[25] T. Yue and M. A. Wahab. "Finite element analysis of fretting wear under variable coefficient of friction and different contact regimes". In: *Tribology International* 107 (2017), pp. 274–282. ISSN: 0301-679X. DOI: https://doi.org/10.1016/j.triboint.2016.11.044.

[26] C. Ruiz, P. H. B. Boddington, and K. C. Chen. "An investigation of fatigue and fretting in a dovetail joint". In: *Experimental Mechanics* 24.3 (1984), pp. 208–217. ISSN: 1741-2765. DOI: 10.1007/BF02323167.

[27] M. J. He and C. Ruiz. "Fatigue life of dovetail joints: Verification of a simple biaxial model". In: *Experimental Mechanics* 29.2 (1989), pp. 126–131. ISSN: 1741-2765. DOI: 10.1007/BF02321364.

[28] P. J. Golden. "Development of a dovetail fretting fatigue fixture for turbine engine materials". In: *International Journal of Fatigue* 31.4 (2009), pp. 620–628. ISSN: 0142-1123. DOI: https://doi.org/10.1016/j.ijfatigue.2008.03.017.

[29] P. Golden and J. Calcaterra. "A fracture mechanics life prediction methodology applied to dovetail fretting". In: *Tribology International* 39.10 (2006). The Fourth International Symposium on Fretting Fatigue, pp. 1172–1180. ISSN: 0301-679X. DOI: https://doi.org/10.1016/j.triboint.2006.02.006.

[30] P. J. Golden and T. Nicholas. "The effect of angle on dovetail fretting experiments in Ti-6Al-4V". In: *Fatigue & Fracture of Engineering Materials & Structures* 28.12 (2005), pp. 1169–1175. DOI: 10.1111/j.1460-2695.2005.00956.x.

[31] R. Neu. "Progress in standardization of fretting fatigue terminology and testing". In: *Tribology International* 44.11 (Oct. 2011), pp. 1371–1377. DOI: 10.1016/j.triboint.2010.12.001.

[32] *ASTM E2789: Guide for Fretting Fatigue Testing.* DOI: 10.1520/e2789-10r15.

[33] S. L. Sunde, F. Berto, and B. Haugen. "Predicting fretting fatigue in engineering design". In: *International Journal of Fatigue* 117 (2018), pp. 314–326. ISSN: 01421123. DOI: 10.1016/j.ijfatigue.2018.08.028.

[34] M. Ciavarella. "A 'crack-like' notch analogue for a safe-life fretting fatigue design methodology". In: *Fatigue & Fracture of Engineering Materials & Structures* 26.12 (2003), pp. 1159–1170. ISSN: 1460-2695. DOI: 10.1046/j.1460-2695.2003.00721.x.

[35] C. Vallellano, J. Domingues, and A. Navarro. "On the estimation of fatigue failure under fretting conditions using notch methodologies". In: *Fatigue & Fracture of Engineering Materials & Structures* 26.5 (2003), pp. 469–478. DOI: 10.1046/j.1460-2695.2003.00649.x.

[36] J. Araújo et al. "On the use of the Theory of Critical Distances and the Modified Wöhler Curve Method to estimate fretting fatigue strength of cylindrical contacts". In: *International Journal of Fatigue* 29.1 (2007), pp. 95–107. ISSN: 0142-1123. DOI: https://doi.org/10.1016/j.ijfatigue.2006.02.041.

[37] J. Araújo et al. "On the prediction of high-cycle fretting fatigue strength: Theory of critical distances vs. hot-spot approach". In: *Engineering Fracture Mechanics* 75.7 (2008). Critical Distance Theories of Fracture, pp. 1763–1778. ISSN: 0013-7944. DOI: https://doi.org/10.1016/j.engfracmech.2007.03.026.

[38] *Abaqus Analysis User's Manual.* URL: http://abaqus.software.polimi.it/v2016/books/usb/default.htm?startat=pt09ch38s02aus184.html (visited on 12/11/2018).

[39] S. Arooj et al. "Effect of Current in the EDM Machining of Aluminum 6061 T6 and its Effect on the Surface Morphology". In: *Arabian Journal for Science and Engineering* 39.5 (2014), pp. 4187–4199. ISSN: 2191-4281. DOI: 10.1007/s13369-014-1020-z.

[40] P. Janmanee et al. "A Study of Surface Hardness Affecting in Electrical Discharge Machining on AISI P20 Plastic Mould Steel". In: *Advanced Materials Research* 557-559 (July 2012), pp. 1791–1796. DOI: 10.4028/www.scientific.net/AMR.557-559.1791.

[41] R. Rajasekaran and D. Nowell. "Fretting fatigue in dovetail blade roots: Experiment and analysis". In: *Tribology International* 39.10 (2006). The Fourth International Symposium on Fretting Fatigue, pp. 1277–1285. ISSN: 0301-679X. DOI: https://doi.org/10.1016/j.triboint.2006.02.044.

[42] D. Hoeppner and V. Chandrasekaran. "Fretting in orthopaedic implants: A review". In: *Wear* 173.1 (1994), pp. 189–197. ISSN: 0043-1648. DOI: https://doi.org/10.1016/0043-1648(94)90272-0.

[43] B. Atzori, G. Meneghetti, and L. Susmel. "Material fatigue properties for assessing mechanical components weakened by notches and defects". In: *Fatigue & Fracture of Engineering Materials & Structures* 28.1-2 (2005), pp. 83–97. DOI: 10.1111/j.1460-2695.2004.00862.x.

[44] K. Kim and A. M. Korsunsky. "Dissipated energy and fretting damage in CoCrAlY-MoS2 coatings". In: *Tribology International* 43.3 (2010), pp. 676–684. ISSN: 0301-679X. DOI: https://doi.org/10.1016/j.triboint.2009.10.007.

[45] D. Swalla and R. Neu. "Influence of coefficient of friction on fretting fatigue crack nucleation prediction". In: *Tribology International* 34.7 (2001), pp. 493–503. ISSN: 0301-679X. DOI: https://doi.org/10.1016/S0301-679X(01)00048-2.

[46] B. Conner and T. Nicholas. "Using a Dovetail Fixture to Study Fretting Fatigue and Fretting Palliatives". In: *Journal of Engineering Materials and Technology-transactions of The Asme - J ENG MATER TECHNOL* 128 (Apr. 2006). DOI: 10.1115/1.2172272.

[47] K. Pereira et al. "On the Convergence of Stresses in Fretting Fatigue". In: *Materials* 9.8 (2016). ISSN: 1996-1944. DOI: 10.3390/ma9080639.

[48] A. Vadiraj and M. Kamaraj. "Characterization of fretting fatigue damage of PVD TiN coated biomedical titanium alloys". In: *Surface and Coatings Technology* 200.14 (2006), pp. 4538–4542. ISSN: 0257-8972. DOI: https://doi.org/10.1016/j.surfcoat.2005.03.036.

A Datasheet Al6082

INSPECTION CERTIFICATE № 16.127613

EN 10204 - 3.1

Consigner: KAMENSK URALSKY METALLURGICAL WORKS JOINT STOCK COMPANY
5, Zavodskaya Str., Kamensk Uralsky, Sverdlovsk Region, 623405, Russia Tel: +7 (3439) 39 54 17 Fax: +7 (3439) 39 57 11

Buyer: ASTRUP AS NORWAY, OSLO	Quantity, pcs: 2
Consignee: ASTRUP NORWAY, OSLO	Net Weight, kg.: 1010
P.O. No.: 1362605 Article No: -	S.O. No.: Z20610 Item No.: 1.3 Package No.: 615319

Description of Goods: Plates

Grade of Product	Dimensions, inch (mm)
40.000X1520.0X3020.0 -	3020 -

Requirements on the Products:

Material conforms to quality of alloy: 6082 T651
-

Product conforms to all requirements of:
EN 485-3:2003; EN 485-1:2010-02; EN 485-2:2013-12; EN 573-3:2013-12

Mechanical Properties

The Condition of Tested Standards	Lot No.	Heat lot No.	HT Charge No.	Sampling direction	Tensile Strength, Rm / Cut MPa		Yield Strength, Rp0,2% / Clenching test MPa		Elongation, %		Hardness, HBW
					min	max	min	max	min	max	
Required				LT	295	-	240	-	8	-	-
-	922383	12-4760	12063	LT	339	339	318	318	8.0	8.0	-

Chemical Composition, %

Element	Silicon Si	Iron Fe	Copper Cu	Manganese Mn	Magnesium Mg	Chromium Cr	Zinc Zn	Titanium Ti	-	-	-
Required	0.7 - 1.3	0.50	0.10	0.40 - 1.0	0.6 - 1.2	0.25	0.20	0.10	-	-	-
Contents	1.0	0.36	0.02	0.6	0.8	0.06	0.01	0.06	-	-	-
Element	-	-	-	-	-	-	-	-	Other Elements Each	Other Elements Total	Aluminum Al
Required	-	-	-	-	-	-	-	-	0.05	0.15	remainder
Contents	-	-	-	-	-	-	-	-	0.05	0.15	remainder

Other Tests

Method	Macro-structure	Micro-structure	UT	K1c	Electro-conductivity,	SCF	Contents H2 of metals cm3/100gr	
					-	-	STP 804.081-2013, MAX 0.25	Raw material used for manufacturing supplied products was tested for compliance with International radiation safety regulations during incoming inspection.
Result	-	-	-	-	-	-	0.19	

On behalf: J.S.Co. "KUMZ"

Date: 14.12.2016

QCB Inspector Ostanina G.A.

Inspection Department Engineer Alekhina N.V.

Astrup AS 06/02/17 klm
1362605/3 5

Al pl 6082-T651 40x1520x3020mm

12-4760

Form № QAD/3-008,Revision 00

B Risk Assessment

NTNU	Hazardous activity identification process	Prepared by	Number	Date
		HSE section	HMSRV2601E	09.01.2013
		Approved by		Replaces
HSE		The Rector		01.12.2006

Unit: **Department of Mechanical and Industrial Engineering** **Date:**

Line manager:

Participants in the identification process: Bjørn Haugen (supervisor), Steffen Loen Sunde (co-supervisor), Andrea Vågen Edvardsen (student)

Short description of the main activity/main process: Master project for student Andrea Vågen Edvardsen. Project title.

Is the project work purely theoretical? (YES/NO): NO *Answer "YES" implies that supervisor is assured that no activities requiring risk assessment are involved in the work. If YES, briefly describe the activities below. The risk assessment form need not be filled out.*

Signatures: *Responsible supervisor:* Bjørn Haugen *Student:* Andrea V. Edvardsen

ID nr.	Activity/process	Responsible person	Existing documentation	Existing safety measures	Laws, regulations etc.	Comment
1	Fatigue lab		Machine's user manual	Room card		
1a	Usage of fatigue lab	AVE	Machine's user manual	Room card		

NTNU	Risk assessment	Prepared by	Number	Date
		HSE section	HMSRV2603E	04.02.2011
HSE/KS		Approved by		Replaces
		The Rector		01.12.2006

Unit: **Department of Mechanical and Industrial Engineering** **Date:** 02.02.19

Line manager: Torgeir Welo

Participants in the identification process: Bjørn Haugen (supervisor), Steffen Loen Sunde (co-supervisor), Andrea Vågen Edvardsen (student)

Short description of the main activity/main process: Master project for student, Andrea Vågen Edvardsen

Is the project work purely theoretical? (YES/NO): NO *Answer "YES" implies that supervisor is assured that no activities requiring risk assessment are involved in the work. If YES, briefly describe the activities below. The risk assessment form need not be filled out.*

Activity from the identification process form	**Potential undesirable incident/strain**	**Likelihood:**	**Consequence:**			**Risk Value (human)**	**Comments/status Suggested measures**
		Likelihood (1-5)	Human (A-E)	Environment (A-E)	Economy/ material (A-E)		
1 Fatigue lab							
1a Usage of the fatigue lab	Crush injury	1	C			C1	Sufficient training before use.
	Flying objects	2	D			D2	Sufficient training before use. Use glasses, place partition in front of machine while running tests
	Damage on eqiptment	2		C	C	C2	Sufficient training before use. Read user manual

Likelihood, e.g.:
1. *Minimal*
2. *Low*
3. *Medium*
4. *High*
5. *Very high*

Consequence, e.g.:
A. *Safe*
B. *Relatively safe*
C. *Dangerous*
D. *Critical*
E. *Very critical*

Risk value (each one to be estimated separately):
Human = Likelihood x Human Consequence
Environmental = Likelihood x Environmental consequence
Financial/material = Likelihood x Consequence for Economy/materiel

Potential undesirable incident/strain

Potential undesirable incident/strain

Identify possible incidents and conditions that may lead to situations that pose a hazard to people, the environment and any materiel/equipment involved.

Criteria for the assessment of likelihood and consequence in relation to fieldwork

Each activity is assessed according to a worst-case scenario. Likelihood and consequence are to be assessed separately for each potential undesirable incident. Before starting on the quantification, the participants should agree what they understand by the assessment criteria:

Likelihood

Minimal 1	Low 2	Medium 3	High 4	Very high 5
Once every 50 years or less	Once every 10 years or less	Once a year or less	Once a month or less	Once a week

Consequence

Grading	Human	Environment	Financial/material
E Very critical	May produce fatality/ies	Very prolonged, non-reversible damage	Shutdown of work >1 year.
D Critical	Permanent injury, may produce serious serious health damage/sickness	Prolonged damage. Long recovery time.	Shutdown of work 0.5-1 year.
C Dangerous	Serious personal injury	Minor damage. Long recovery time	Shutdown of work < 1 month
B Relatively safe	Injury that requires medical treatment	Minor damage. Short recovery time	Shutdown of work < 1week
A Safe	Injury that requires first aid	Insignificant damage. Short recovery time	Shutdown of work < 1day

The unit makes its own decision as to whether opting to fill in or not consequences for economy/materiel, for example if the unit is going to use particularly valuable equipment. It is up to the individual unit to choose the assessment criteria for this column.

Risk = Likelihood x Consequence

Please calculate the risk value for "Human", "Environment" and, if chosen, "Economy/materiel", separately.

About the column "Comments/status, suggested preventative and corrective measures":

Measures can impact on both likelihood and consequences. Prioritise measures that can prevent the incident from occurring; in other words, likelihood-reducing measures are to be prioritised above greater emergency preparedness, i.e. consequence-reducing measures.

MATRIX FOR RISK ASSESSMENTS at NTNU

CONSEQUENCE						
	Extremely serious	E1	E2	E3	E4	E5
	Serious	D1	D2	D3	D4	D5
	Moderate	C1	C2	C3	C4	C5
	Minor	B1	B2	B3	B4	B5
	Not significant	A1	A2	A3	A4	A5
		Very low	Low	Medium	High	Very high
		LIKELIHOOD				

Principle for acceptance criteria. Explanation of the colours used in the risk matrix.

Colour		Description
Red		Unacceptable risk. Measures must be taken to reduce the risk.
Yellow		Assessment range. Measures must be considered.
Green		Acceptable risk Measures can be considered based on other considerations.

NTNU

Norwegian University of
Science and Technology